Chapter 12

Four-Wave Mixing in Single-Mode Optical Fibers

Alex McMillan[*], Yu-Ping Huang[†], Bryn Bell1[*], Alex Clark[‡], Prem Kumar[†] and John Rarity[*]

[*] *Photonics Group, Merchant Venturers School of Engineering, University of Bristol, Bristol, BS8 1UB, UK*

[†] *Center for Photonic Communication and Computing, Department of Electrical Engineering and Computer Science & Department of Physics and Astronomy, Northwestern University, 2145 Sheridan Road, Evanston, Illinois 60208, USA*

[‡] *Centre for Ultrahigh Bandwidth Devices for Optical Systems (CUDOS), Institute of Photonics and Optical Science (IPOS), School of Physics, University of Sydney, NSW 2006, Australia*

Chapter Outline

12.1 Introduction 412
12.2 Photon Pair Generation in Optical Fibers 413
12.2.1 Classical Four-Wave Mixing Theory and Phase-Matching Requirements 413
12.2.2 Quantum Theory of Four-Wave Mixing 416
12.2.3 Cross-Polarized Four-Wave Mixing in Birefringent Fibers 419
12.2.4 Raman Scattering 420
12.3 Heralded Single-Photon Sources Based on sFWM 422
12.3.1 Photon-Pair Generation in the Anomalous Dispersion Regime 425
12.3.2 Photonic Crystal Fiber Sources in the Normal Dispersion Regime 427
12.4 Quantum Interference Between Separate Spectrally Filtered Fiber Sources 430
12.5 Intrinsically Pure-State Photons 436
12.5.1 Generation of Spectrally Uncorrelated Two-Photon States Through Group Velocity Matching 436
12.5.2 A Temporal Filtering Approach for Attaining Pure-State Photons 440
12.6 Entangled Photon-Pair Sources 444
12.7 Applications of Fiber Photon Sources—All-Fiber Quantum Logic Gates 454

Single-Photon Generation and Detection, Volume 45. http://dx.doi.org/10.1016/B978-0-12-387695-9.00012-3

12.8 Photonic Fusion in Fiber 458
12.9 Conclusion 460
References 461

12.1 INTRODUCTION

In many ongoing experiments in quantum information, probabilistic photon sources based on the generation of photon pairs using nonlinear optics have proven to be an excellent approach, due to their typically high brightness and the wide range of photon properties that can be attained in different nonlinear systems. Photon sources based on spontaneous parametric down-conversion in bulk $\chi^{(2)}$ nonlinear crystals, and more recently waveguides in $\chi^{(2)}$ materials (see Chapter 11), are still the most commonly used, but in recent years there has been much interest in sources based on parametric photon pair generation in optical fibers.

In optical fibers the $\chi^{(3)}$ nonlinear response of the silica glass core can lead to the generation of correlated pairs of photons, known as the signal and idler, through spontaneous four-wave mixing when either a single intense pump field, or pump fields at two distinct wavelengths are propagating in the fiber. This process can only occur efficiently when the constraints of both energy and momentum conservation (i.e., phase-matching) of the optical fields are satisfied. The spectral properties of the photon pairs that can be generated are largely dependent on the dispersion properties of the fiber. When pumping close to the zero-dispersion wavelength of a fiber, depending on the exact choice of pump wavelength, phase-matching can be satisfied for either widely separated signal and idler photon pairs [1], or for signal and idler pairs generated close to the pump wavelength [2].

Even greater flexibility can be achieved for four-wave mixing in photonic crystal fiber, in which the dispersion can be tailored through design of the fiber structure. Pair photon generation has been demonstrated in photonic crystal fiber using a wide range of different pump sources with generated photons covering a considerable wavelength range, from the visible to telecom wavelengths in the near infrared, making them suitable for a wide range of applications [3–7]. Through careful design of the fiber structure it is also possible to influence other properties of the photon pair, in order to generate them on a well-defined polarization axis of the fiber and to avoid undesirable spectral correlations between the signal and idler photons which must otherwise be eliminated through lossy, narrowband spectral filtering [8–10].

Although the generation of photon pairs by four-wave mixing is probabilistic in nature, the photons are always produced simultaneously in pairs, so the detection of one photon can be used to herald the presence of the other. Such fiber-based heralded single-photon sources have been demonstrated with high brightness (generated pair probability) due to the long nonlinear interaction

lengths that can be achieved in a waveguide configuration, with the pump beam confined to a small mode area. Furthermore, as the photons can be generated in the fundamental guided mode of the fiber, they can be coupled into standard single-mode fiber with high efficiency. This has led to the development of spliced all-fiber sources with very low optical losses and high stability [5,11,12]. The ease of integration of these photon sources with standard fiber-based optical components has also been crucial for demonstrations of all-fiber quantum logic gates [13].

In addition to heralded single photons, fiber-based photon sources can be designed to generate useful two-photon states. Of particular interest are polarization-entangled signal and idler pairs, which can be generated via various schemes [14–16]. Looking beyond two-photon entangled states, larger entangled cluster states have now been demonstrated by linking the states output from multiple fiber-based photon sources through selective measurement of the output photons [17]. As these states can be used as a resource for universal quantum computation [18], the generation of larger cluster states and investigation into their properties is an area of great future interest.

12.2 PHOTON PAIR GENERATION IN OPTICAL FIBERS

12.2.1 Classical Four-Wave Mixing Theory and Phase-Matching Requirements

Four-wave mixing (FWM) is a third-order nonlinear ($\chi^{(3)}$) optical process that occurs naturally in all optical materials, including fibers, in which an intense, propagating pump field provides amplification for light fields at other wavelengths. In many ways, the process is similar to parametric down-conversion in second-order nonlinear ($\chi^{(2)}$) crystals, which has been widely studied for use as the basis of single-photon sources. FWM results from the coupling of light fields at four distinct wavelengths (in the most general case) due to the polarization response of the transmission medium in which the light is propagating. The polarization response $\mathbf{P}$ of a material in the presence of light with an electric field component $\mathbf{E}$ can be described by

$$\mathbf{P} = \epsilon_0(\chi^{(1)} \cdot \mathbf{E} + \chi^{(2)} : \mathbf{EE} + \chi^{(3)} \vdots \mathbf{EEE} + \cdots), \tag{12.1}$$

where the $\chi^{(j)}$ terms are the jth order coefficients of a Taylor series expansion of the electric susceptibility of the material [19]. In isotropic materials, such as a silica glass, there will be no $\chi^{(2)}$ term because of symmetry constraints, and the nonlinear response of the material is dominated by the $\chi^{(3)}$ contribution. In addition to effects such as third harmonic generation and self-phase modulation, the $\chi^{(3)}$ nonlinear response allows FWM, where two intense optical fields (pump fields of angular frequency ω_{p1} and ω_{p2}) lose energy and provide gain for two other fields (the so called signal at higher frequency ω_s and the idler at the

lower frequency ω_i). Most commonly, the two pump fields are chosen to be degenerate in frequency (ω_p), such that the process can be pumped using a single high-power laser. If a probe beam at the signal or idler wavelength is also launched with the pump it will be amplified (a phase-insensitive process), and result in the generation of light at the other wavelength. When both the signal and idler modes are initially empty, spontaneous four-wave mixing (sFWM) can occur, with the process seeded by quantum vacuum noise. In this case the signal and idler appear in the spectrum as newly generated sidebands, equally spaced in frequency about the central pump peak.

At the quantum level the sFWM process can be regarded as the virtual absorption of two pump (p) photons and subsequent creation of a signal (s) and idler (i) photon pair. As the response time of the $\chi^{(3)}$ Kerr nonlinearity in optical fibers is nearly instantaneous, this allows the detection of one photon of the pair to herald the generation of the other. For a given fiber structure and pump laser, the signal and idler wavelengths that will be generated through sFWM are determined by the energy and phase-matching conditions:

$$2\omega_p = \omega_s + \omega_i, \tag{12.2}$$

and

$$\kappa = k_s + k_i - 2k_p + 2\gamma P_p. \tag{12.3}$$

Here κ is the phase-mismatch between the propagation constants of the signal, idler, and pump waves resulting from chromatic dispersion, with $k_j = \frac{n_j \omega_j}{c}$ ($j = s,i,p$) for light with angular frequency ω_j propagating in a medium with refractive index n_j at that frequency. Only when the phase-mismatch is near zero will the average probability of generated signal and idler photon pairs increase along the entire length of the fiber and build up to appreciable levels. The $2\gamma P_p$ term in Eq. (12.3) is the correction to the phase-mismatch due to self-phase modulation of the intense pump pulse, where P_p is the peak pump power and γ is the nonlinear coefficient of the fiber, given by

$$\gamma = \frac{2\pi n_2}{\lambda_p A_{\text{eff}}}. \tag{12.4}$$

The nonlinear coefficient of a fiber is determined by the pump wavelength λ_p, the effective cross-sectional area of the fiber mode A_{eff} and the nonlinear refractive index of the material n_2. For silica, $n_2 = 2 \times 10^{-20}$ m^2/W [19].

Figure 12.1 shows an example of a phase-matching curve, calculated for a typical fiber using Eqs. (12.2) and (12.3) at different pump powers. Two different regimes of light propagation can be identified on this figure. At short wavelengths the fiber exhibits normal dispersion, where longer wavelength components of a light pulse travel faster than shorter wavelength components. At longer wavelengths the dispersion is anomalous and the situation is reversed. At the boundary between these regions is the zero-dispersion wavelength, where

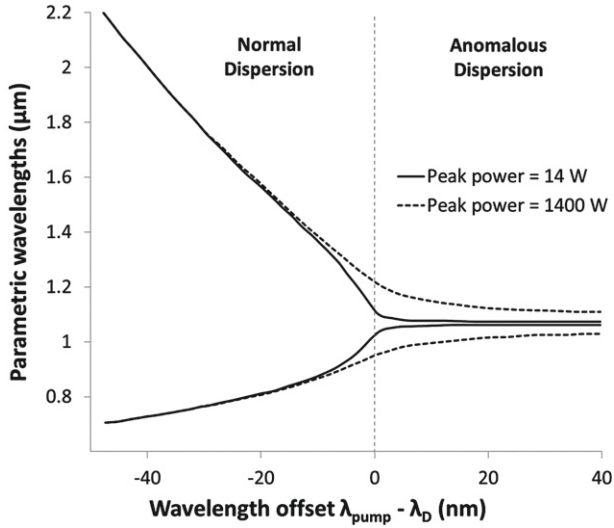

FIGURE 12.1 Calculated phase-matching curves for sFWM in an optical fiber at two different levels of peak pump power. The generated signal and idler wavelengths are shown for pump laser wavelengths λ_{pump} close to the zero-dispersion wavelength λ_D. This phase-matching curve is for a photonic crystal fiber, in which the zero-dispersion wavelength has been shifted toward the visible regime compared to conventional single-mode fibers. *Image adapted from [20].*

the dispersion parameter D of the fiber is zero, such that

$$D = -\frac{2\pi c}{\lambda^2}\frac{d^2k}{d\omega^2} = 0. \tag{12.5}$$

The behavior of the phase-matching conditions for sFWM depends on whether the pump wavelength is above or below the zero-dispersion wavelength. In the anomalous regime, $2k_p > k_s + k_i$, so for signal and idler wavelengths close to the pump the nonlinear self-phase modulation term $+2\gamma P_p$ can be used to compensate for the phase-mismatch. This results in broad sidebands close to the pump wavelength, with their separation highly dependent on the pump power P_p. However, in the normal dispersion regime where $2k_p < k_s + k_i$, the nonlinear term increases the phase-mismatch. Here higher order dispersion terms become important and phase-matching can be achieved close to the zero-dispersion wavelength for large detuning of the signal and idler wavelengths from the pump. In the normal dispersion region the phase-matched signal and idler wavelengths are not strongly affected by the pump power, but can vary considerably in response to small changes in the pump wavelength.

In conventional fibers, the refractive index contrast between the core and cladding that is required for guidance is attained by doping the glass in either the core or cladding regions. As this index contrast is relatively weak, the dispersion properties of conventional fibers are predominantly determined by the inherent material dispersion of bulk silica, with a zero-dispersion wavelength

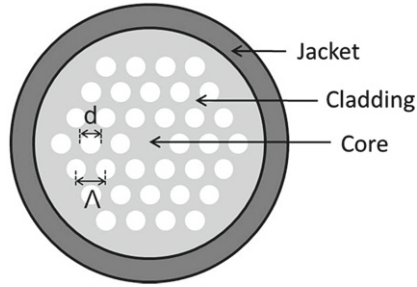

FIGURE 12.2 Schematic representation of a simple photonic crystal fiber design, based on a triangular lattice. The core region is solid silica, while the cladding is formed by a periodic array of air holes. The properties of the fiber are determined by the hole diameter (d) and pitch (Λ).

near 1.3 μm. While it is possible to modify dispersion in conventional fibers with a structured cladding index profile, the extent to which the zero-dispersion wavelength can be moved is limited and it cannot be easily shifted to shorter wavelengths [21].

An alternative approach to sFWM in conventional all-solid fiber is to take advantage of the additional design flexibility available in photonic crystal fiber (PCF). For PCF the fiber is produced from a single material, typically pure silica. In PCF structures designed for photon pair generation through sFWM, the nonlinear interaction occurs in a solid silica core, while the cladding region is formed from a periodic array of air holes in the silica, which run along the length of the fiber (see Fig. 12.2). The presence of the air holes can reduce the effective index of the cladding significantly compared to the solid silica core, leading to stronger guidance than in conventional fibers. Unlike in conventional fibers, the waveguide contribution to dispersion can therefore be of a similar magnitude to the inherent material dispersion, either compensating it or enhancing it depending on the PCF structure.

Physical realizations of various photon sources based on conventional fibers and PCF, and operating with pumping in both the normal and anomalous dispersion regimes are discussed in Section 12.3.

12.2.2 Quantum Theory of Four-Wave Mixing

In order to better understand the properties of the photon-pair state that is generated through sFWM, it is useful to extend the theoretical model described in Section 12.2 to incorporate quantization of the signal and idler modes [22–24]. Commonly a semi-classical approach is taken, in which the bright pump beam is treated using classical nonlinear optics, but its interaction with the signal and idler fields is implemented using photon creation operators $\hat{a}_s^\dagger$ and $\hat{a}_i^\dagger$ acting on an initially empty vacuum state. The nonlinear interaction Hamiltonian associated with the sFWM process (assuming phase-matching is

satisfied, and that sFWM occurs in a single temporal, spatial, and polarization mode) is of the form

$$H_{\text{int}} = g(\hat{a}_s^\dagger \hat{a}_i^\dagger + \hat{a}_s \hat{a}_i). \tag{12.6}$$

The first term in Eq. (12.6) corresponds to the creation of a correlated signal and idler pair, achieved through the annihilation of two pump photons (although this is not shown due to the undepleted pump approximation wherein the back effect of sFWM on the pump is neglected; see, e.g., [25]). The second term is the reverse process, by which a signal and idler photon can be converted to two photons at the pump wavelength. The coupling coefficient g determines the strength of the interaction and incorporates several parameters, most notably the intrinsic nonlinear susceptibility of the material $\chi^{(3)}$, the peak power of the pump laser and the effective mode field area of the fiber. The nonlinear response is enhanced for small core fibers where the pump light is tightly confined.

Using the interaction Hamiltonian shown in Eq. (12.6), and assuming for now that the sFWM process described allows generation of signal and idler photons only in the single-mode regime, the generated state is given by

$$|\psi_{\text{out}}\rangle \propto |vac\rangle + \alpha|1,1\rangle_{s,i} + \alpha^2|2,2\rangle_{s,i} + \cdots, \tag{12.7}$$

where $|\alpha|^2$ is the average number of photon pairs generated per temporal mode, $|vac\rangle$ is the vacuum component of the state containing no pairs, and the first and second numbers in each of the other state components denote the number of generated signal and idler photons respectively. Because of the stochastic nature of spontaneous parametric processes, the output signal and idler states prior to measurement consist of a series of terms with increasing photon number and increasing powers of α. However, because the number of photons in the signal and idler modes must be perfectly correlated (in the absence of loss), measurement of either the signal or idler state can be used to determine when the desired number state of photons in the other frequency mode was successfully generated. This can be used to realize heralded single-photon sources, as described in Section 12.3.

The energy and phase-matching requirements identified in Eqs. (12.2) and (12.3) may seem to imply that unique, monochromatic solutions for the signal and idler fields exist for any chosen pump wavelength. While these conditions do define the peak signal and idler wavelengths that are generated, in reality there will always be some finite bandwidth associated with these fields. The requirements for producing spectrally pure-state photons place stringent conditions on the bandwidth of the generated photons, which generally means that they must be spectrally filtered. This is described in detail in Section 12.4. Understanding the factors influencing the gain bandwidth for sFWM is therefore important, as this determines the proportion of the generated photon pairs that will be produced within the desired spectral range.

By using a truncated Taylor expansion of the wavevector terms in the phase-matching equation (Eq. (12.3)) it can be shown [22] that the full-width

half-maximum (FWHM) bandwidths of the signal and idler fields, $\Delta\omega_s$ and $\Delta\omega_i$, are given by

$$\Delta\omega_s = \frac{2\pi c}{|\mathcal{N}_s - \mathcal{N}_i|L} + 2\left|\frac{\mathcal{N}_i - \mathcal{N}_p}{\mathcal{N}_s - \mathcal{N}_i}\right|\Delta\omega_p, \tag{12.8}$$

and

$$\Delta\omega_i = \frac{2\pi c}{|\mathcal{N}_i - \mathcal{N}_s|L} + 2\left|\frac{\mathcal{N}_s - \mathcal{N}_p}{\mathcal{N}_i - \mathcal{N}_s}\right|\Delta\omega_p, \tag{12.9}$$

where $\Delta\omega_p$ is the FWHM bandwidth of the pump, L is the length of the fiber, and $\mathcal{N}_j$ ($j = s,i,p$) are the group indices for the signal, idler, and pump, given by $\mathcal{N}_j = (\omega_j \frac{\partial n_j}{\partial\omega}\Big|_{\omega_j} + n_j)$. The first terms in Eqs. (12.8) and (12.9) show the bandwidth that exists even in the case of a monochromatic pump, due to the finite length of the fiber. As L is increased the tolerance of the sFWM process to phase-mismatch is reduced, and the bandwidth over which signal and idler photons are generated is consequently also reduced.

Working in the interaction picture of quantum mechanics it is also possible to use the Hamiltonian described in Eq. (12.6) to calculate the average number of photon pairs that will be generated by sFWM, which is useful for predicting the attainable brightness of photon sources based on this process. When using a pulsed laser as a pump source, the average number of generated signal photons per pulse $\langle N_s\rangle$ is [22]

$$\langle N_s\rangle = \left(\frac{SIL}{2}\right)^2 \left(\frac{\pi\Delta\omega_p^2}{4\ln(4)}\right)^{3/2} \left(\frac{4\sqrt{2}\pi c}{(\mathcal{N}_s - \mathcal{N}_i)L}\right)\frac{\mathcal{N}_s\mathcal{N}_i}{c^2}, \tag{12.10}$$

where I is an overlap integral between the spatial mode profiles of the signal, idler, and pump fields and S is a gain coefficient term given by

$$S = \epsilon_0\chi^{(3)}\frac{E_{p0}^2}{4}\sqrt{\frac{\omega_s\omega_i}{4\epsilon_s\epsilon_i}}, \tag{12.11}$$

where E_{p0} is the peak electric field amplitude of the pump pulse. The expression for the mean value of generated idler photons per pulse is identical, as expected since the signal and idler photons are always generated together in pairs. As shown in Eq. (12.10), the expectation value for the number of generated pairs depends on the strength of the nonlinearity of the fiber (through $\chi^{(3)}$) and on the square of the peak pump power. The total number of generated pairs increases linearly with the fiber length L. However, when considering only those generated photons that fall within a narrow spectral range, which is small compared to the gain bandwidth (as is often the case for photon sources which rely on narrowband spectral filtering to achieve purity), the increase in fiber length not only increases the total number of generated pairs, but also reduces the gain bandwidth, as shown in Eqs. (12.8) and (12.9). Because of this, the number of useful photon pairs falling within the selected narrow bandwidth

grows with the square of the fiber length in this case, as long as the total fiber length does not exceed the pulse walk-off length, the length over which two initial co-propagating pulses become spatially separated [19].

12.2.3 Cross-Polarized Four-Wave Mixing in Birefringent Fibers

In addition to the co-polarized sFWM process described so far, where the pump, signal and idler fields have the same polarization state, phase-matching can also be achieved for cross-polarized spontaneous four-wave mixing. For this process the signal and idler are both generated in a polarization state which is orthogonal to that of the pump. Due to the material symmetry of silica, the relevant nonlinear electric susceptibility coefficient for this process $\chi^{(3)}_{xxyy}$ is only $\frac{1}{3}$ that of the co-polarized process $\chi^{(3)}_{xxxx}$, where x and y define two orthogonal transverse polarization axes of the fiber. The first two terms in the subscript correspond to the polarization state of the pump fields and the third and fourth terms refer to the polarization state of the signal and idler photons [25].

Although the gain for cross-polarized sFWM is inherently lower, in birefringent fibers this process is of considerable interest, as the strength of the birefringence provides an additional parameter that can be used to tailor the fiber dispersion in order to satisfy the phase-matching requirements. A fiber with birefringence exhibits a difference in its refractive index depending on whether light propagates on the fast or slow axis of the fiber. Birefringence in standard index guiding all-solid fibers is usually implemented by the introduction of stress applying elements close to the core, producing an asymmetric refractive index profile across the core region. In strongly birefringent fibers this can provide a difference in refractive index between the fast and slow axis $\delta n \sim 10^{-4}$. In PCF, asymmetry can alternatively be introduced in the geometry of the fiber structure, for instance by slightly collapsing or expanding one of the cladding air holes on either side of the core leading to an elliptical mode field profile [26]. Form-induced birefringence of this type can achieve $\delta n > 10^{-3}$ in the case of a highly elliptical core [27].

The phase-matching requirements shown for co-polarized sFWM in Eq. (12.3) can be modified to describe the cross-polarized sFWM process, in which pump light launched onto one axis of the fiber, generates signal and idler pairs on the orthogonal axis. The effective mode indices for the signal and idler $n_{s,i}$ are modified by an additional term δn to account for propagation on a different axis to the pump, with the sign of the contribution dependent on which axis of the fiber is pumped, such that

$$n_{s,i}(\lambda) = n_p(\lambda) \pm \delta n. \tag{12.12}$$

The strength of the birefringence can be selected to provide phase-matching for a desired set of operating wavelengths in a similar manner to the $2\gamma P_p$ term in Eq. (12.3) although even in weakly birefringent structures, the magnitude of the δn term is usually far more significant, and can help to achieve phase-matching in both the anomalous and normal dispersion regimes relatively far from the

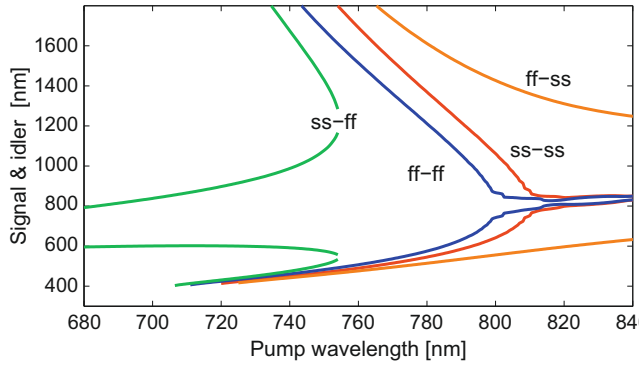

FIGURE 12.3 Phase matching curve for FWM in birefringent PCF. The curves ff–ff and ss–ss represent the phase-matching cases where pump and generated photons are all polarized along the fast or slow axes respectively. In the case of ff–ss and ss–ff, the pump photons are polarized orthogonally to the signal and idler. *Image from [10].*

zero-dispersion wavelength. As shown on the example phase-matching plot in Fig. 12.3, this allows for generation of signal and idler photons on the fast axis of the fiber when the pump is propagating on the slow axis in the normal dispersion regime (ss $\rightarrow$ ff), or for generation of photons on the slow axis when pumping on the fast axis in the anomalous dispersion region (ff $\rightarrow$ ss). The separation of the signal and idler wavelengths from the pump increases with strength of the birefringence. Of particular interest are the turning points on the phase-matching plot where the gradient of either the signal or idler curve become zero. At these points either the signal or idler photons will be generated within a very narrow spectral range, which can be anticipated from Eqs. (12.8) and (12.9). It will be shown in Section 12.5.1 that the states of the generated signal and idler photons become spectrally uncorrelated in these regions, leading to two-photon states with highly desirable properties for use in photon sources.

12.2.4 Raman Scattering

The performance of fiber-based photon source is often limited by the detection of uncorrelated noise photons arising from processes other than the desired sFWM interaction. One such source of noise is the nonlinear shift in the energy of photons, predominantly to longer wavelengths, due to spontaneous Raman scattering. When bright laser light from a pump source propagates in an optical fiber, the Raman effect allows photons at the pump wavelength to be inelastically scattered by the silica glass, resulting in the emission of a phonon, and a photon with a red-shifted frequency. This leads to an increase in the background count rates measured for fiber-based photon sources when the wavelength of the Raman-shifted pump light overlaps with the idler wavelength generated through sFWM.

The shift in frequency associated with Raman scattering depends on the phonon distribution, which is characteristic of the material. Due to the amorphous nature of silica, the energy range of phonons in the material is

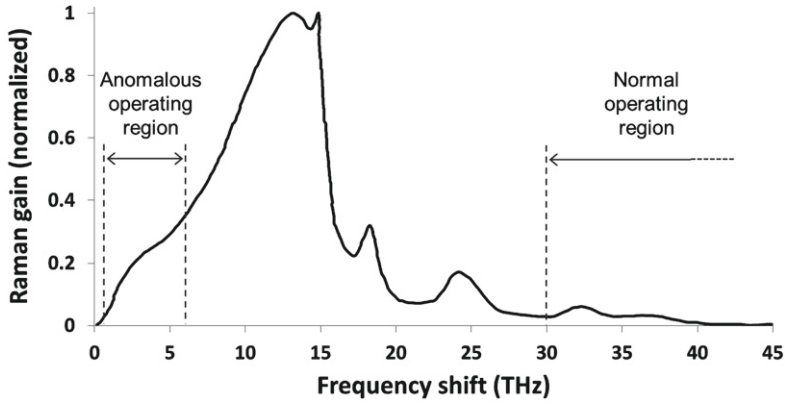

FIGURE 12.4 Normalized gain spectrum for Raman-shifted pump light in silica [19]. The range of idler frequencies (given as an offset from the pump) previously demonstrated for photon sources in the anomalous and normal dispersion regimes of fiber is overlaid (see Sections 12.3.1 and 12.3.2). *Image adapted from [19].*

distributed in a wide and continuous band. The Raman gain peaks for a frequency shift of 13 THz and reduces significantly for larger frequency shifts as well as very close to the original pump wavelength, as shown in Fig. 12.4. For photon sources operating in the anomalous dispersion regime, where the signal and idler wavelengths are constrained to lie close to the pump due to the phase-matching conditions, the Raman contribution can be reduced by minimizing the offset between the pump and idler. For sources pumped in the normal dispersion regime, the signal and idler are generally widely separated, such that the idler wavelength can lie beyond the extent of the Raman gain. In either case, the use of pump pulses with relatively high peak power can help to reduce the effect of Raman noise, as the generation rate of photon pairs through sFWM is proportional to the peak pump power squared, whereas Raman generation increases linearly with the pump intensity and fiber length in the low power regime of interest [28]. However, this effect comes at the price of increased background emission of multiple photon pairs, introducing impurity to the photon-pair state produced. Raman scattering can also be suppressed by cooling of the fiber with liquid nitrogen to reduce the phonon population [29].

Another viable approach to mitigate the Raman scattering effect is to apply on the output photons mode-selective filtering that is capable of discriminating the Raman-scattered photons from the paired photons, even if they are of the same wavelength [30]. It is known that Raman scattering in optical fibers occurs with a time-retarded response to the intense pump fields, while the sFWM occurs in a nearly instantaneous response. As a result, when short-duration pump pulses are applied, the Raman photons will be produced in a mixture of temporal modes different from the photon pairs. The idea is then to construct a temporal-shaped filter such that only a single mode of the photon pairs can pass through. All other modes will be rejected, thereby filtering out most of the Raman photons.

The effectiveness of this method depends on the mode overlap between the photon pairs and the Raman photons. Using this approach, Huang *et al.* found numerically that the quantum-state purity of entangled photons generated in room-temperature fibers can be improved significantly from 82% to 95% in terms of the two-photon Hong-Ou-Mandel interference visibility [30].

12.3 HERALDED SINGLE-PHOTON SOURCES BASED ON sFWM

An ideal single-photon source would emit photons sequentially, such that each output time bin of the source contained one (and only one) photon in a desired pure quantum state. For the case of a pulsed pump, each pulse defines a single time bin which should ideally contain a single output photon. For a CW photon source, the width of the time bins is given by the coherence time of the generated photon state. As is the case with photon sources based on parametric down-conversion in $\chi^{(2)}$ crystals, the advantage of a single-photon source based on sFWM over a weak coherent state arises from the fact that the signal and idler photons are always generated together in correlated pairs. The detection of one photon of the pair can be used to infer the presence of the other, a procedure known as heralding (see Fig. 12.5) [31]. Heralding removes the vacuum contribution to the generated state in which no pairs are generated, which is seen in Eq. (12.7).

While heralding removes the vacuum contribution of the generated state, higher order terms in which multiple photon pairs are generated will still be present due to the probabilistic nature of pair generation. However, if the probability of generating a signal and idler pair in any given time bin is low (when α is small in Eq. (12.7)), the contribution of such higher order terms to the generated state can be made arbitrarily small. The requirement of keeping the pair generation rate low imposes a fundamental limit on the brightness of the source that can be achieved. In the case of a pulsed pump, the pump power is

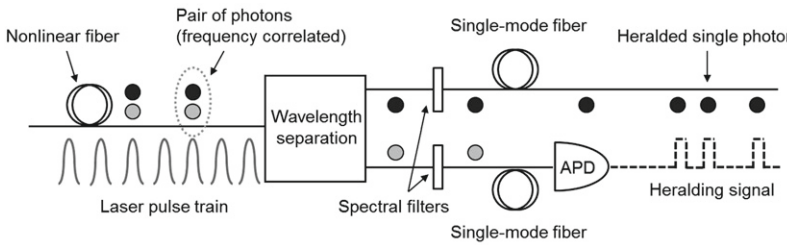

FIGURE 12.5 Typical experimental arrangement of a fiber-based heralded photon source. Pairs of signal and idler photons are generated in a section of nonlinear fiber before being separated by wavelength and filtered to attain spectral purity. After coupling into separate output fibers, one member of the pair is detected using a single-photon avalanche photodiode (SPAD) to herald the presence of the other. *Image from [32].*

typically chosen to provide a pair generation probability of 0.1 pairs per pulse, or less if high quantum-state purity is desirable. Given this limitation, a high repetition rate pump laser is usually desirable, to maximize the generation rate of photon pairs.

The brightness of the source is commonly defined as the number of heralded single photons output from the source per second, which for the purposes of characterizing such sources is often given as a measured twofold coincidence count rate between signal and idler photons (with units of s^{-1}). The measured coincidence count rate is given by

$$C = r\eta^{s}_{\text{opt}}\eta^{i}_{\text{opt}}\eta^{s}_{\text{DE}}\eta^{i}_{\text{DE}} + C_a, \tag{12.13}$$

where r is the rate of photon-pair generation in the fiber, $\eta^{s,i}_{\text{DE}}$ are the efficiencies of the detectors for the signal and idler photons, and $\eta^{s,i}_{\text{opt}}$ are the optical transmission efficiencies for the signal and idler, which incorporates all sources of loss between the point at which the photons are generated and the detectors. C_a are accidental coincidence counts arising from all uncorrelated detection events.

Alternative commonly used definitions of the brightness include the coincidence count rate per unit pump power (s^{-1} mW^{-1}) and per unit bandwidth of the generated photon pairs (s^{-1} mW^{-1} nm^{-1}). However, due to the nonlinear relation between the photon pair generation rate and the pump power, the natural units to measure source brightness should depend on the square of the pump power (s^{-1} mW^{-2} or s^{-1} mW^{-2} nm^{-1}). Such measures aim to highlight both the efficiency of the nonlinear process (through pump power requirements) and the proportion of the generated photon pairs that fall within the useful spectral range (as such sources typically require narrowband spectral filtering to be applied to the signal and idler after generation). As the pump power requirements and bandwidth of the sFWM gain spectrum can be influenced by many factors, such as pump pulse duration and repetition rate, the wavelengths of interest, and properties of the fiber in question, these factors must be taken into account when assessing the brightness of competing sources.

As previously described, there is an inevitable trade-off between the brightness of the source and the detrimental contribution to the output state of multiple pair generation events. The latter can be quantified using the so-called coincidence-to-accidental ratio (CAR). As the signal and idler photons are always generated together in pairs, by selecting the delay between measurement of the signal and idler channels appropriately (to account for any difference in the path length to the detectors for the two photons) the coincident detection rate between photons generated in correlated pairs, on the same pulse of the pump laser, can be observed. In contrast, the accidental rate can be found by selecting the delay between detectors such that coincident detections between the signal photons generated on one pulse of the pump laser and photons at the idler wavelength generated on a subsequent (or preceding) pulse of the pump laser are observed (see Fig. 12.6). These accidental twofold coincidences are a

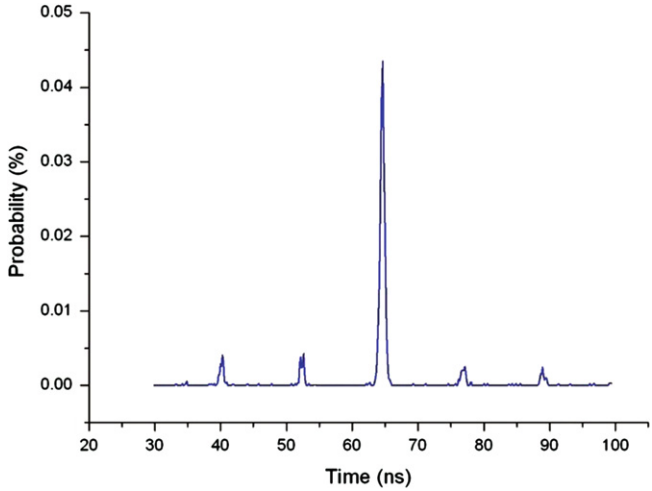

FIGURE 12.6 Typical measured twofold coincident count rate data between signal and idler photons. The histogram shows the probability that a heralded photon will be detected given that a heralded signal was produced, as function of the time delay between the detections. The large central peak arises from the detection of correlated photon pairs, while the smaller satellite peaks are separated by the laser repetition rate and indicate the background uncorrelated accidentals contribution to the count rate. *Image from [3].*

source of noise in the system which can be present on any pulse of the pump laser (including those in which a heralding signal is generated).

The accidental count rate is due to detections events which are uncorrelated with the heralding signal and can be made up of contributions from several sources. These include residual pump photons which pass through the spectral filtering in the source and reach the detectors, Raman-shifted pump light (primarily at the idler wavelength) and detector dark counts. The other main contribution to the accidentals count rate comes from the generation of additional photon pairs through sFWM that are uncorrelated with the pair that caused the heralding signal. While the other noise sources can be minimized, the accidentals count rate due to multiple pair generation is unavoidable and, when other sources of noise are negligible, limits the CAR to 10 when the source is operated at the typical pair generation rate of 0.1 pairs per pulse.

In addition to the CAR, the heralding efficiency is another important figure of merit for a single-photon source. The heralding efficiency H is the probability that a photon will be output from the source, given that a heralding signal was detected and is given by

$$\eta_{\text{herald}} = \frac{C - C_a}{R_{\text{h}}\eta_{\text{det}}}, \tag{12.14}$$

where C is the measured coincidence count rate for correlated signal and idler photons, C_a is the accidentals count rate, R_{h} is the measured singles count rate for the heralding photons, and η_{det} is the efficiency of the detector

used to measure the output heralded photons. η_{herald} is closely related to the transmission efficiency of the device at the peak output wavelength. However, it may deviate from this value in the case of narrowband filtering, where edge effects can occur due to the profile of the spectral filtering. η_{herald} can also be reduced by uncorrelated noise photons in the heralding channel, leading to an erroneously high singles count rate R_{h}. To maximize the heralding efficiency it is therefore essential to keep the optical loss in the output photon channel of the source as low as possible. As seen in Eq. (12.13), the brightness of the source will also be improved by minimizing the loss for both the signal and idler photons.

12.3.1 Photon-Pair Generation in the Anomalous Dispersion Regime

Due to the requirement of phase-matching, when pumping in the anomalous dispersion regime of an optical fiber the central wavelengths of the generated signal and idler will depend on the peak power of the pump beam. For generation of single photons in the signal and idler modes, the required peak pump power is relatively low, leading to signal and idler wavelengths separated from the pump wavelength by typically a few tens of nanometers.

The earliest demonstrations of heralded single-photon generation in optical fiber focused on sFWM in the anomalous dispersion regime of dispersion-shifted conventional fibers (DSF), and are reported in [2,33]. By using a 300 m length of fiber with a zero dispersion wavelength shifted to 1535 nm, and pumping using 5 ps pulses at 1536 nm from an optical parametric oscillator, Li *et al.* were able to generate correlated pairs of signal and idler photons at 1532 and 1540 nm respectively (see Fig. 12.7) [33].

This early work highlighted some of the key advantages of fiber-based photon sources. Firstly, despite the relatively weak $\chi^{(3)}$ nonlinear response of silica glass, efficient photon generation can occur at modest pump powers due to the long interaction lengths that can be realized, due to the confinement of the optical mode to the fiber core along the entire fiber length. Secondly, by selecting a fiber with the appropriate dispersion characteristics, phase-matching for the desired signal and idler wavelengths can be achieved without the need for angle and temperature tuning that is often required for photon sources based on parametric down-conversion in bulk $\chi^{(2)}$ crystals. In addition, generating the photon pair directly in the guided mode of a fiber allows the heralded single-photon state to be easily prepared in a single spatial mode. For $\chi^{(2)}$ crystal-based sources, collection of the generated photons into single-mode fiber remains one of the main sources of optical loss, with schemes to improve the collection efficiency often relying on delicate or complex alignment. In the case of optical fiber-based sources, fusion splicing can easily allow sections of conventional fiber to be joined with negligible loss (typically <0.1 dB).

Parallel to the use of standard single-mode fibers, photonic-crystal fibers with relatively large Kerr nonlinearity have also been commonly used to create correlated and entangled photon pairs. An advantage offered by PCFs is that they

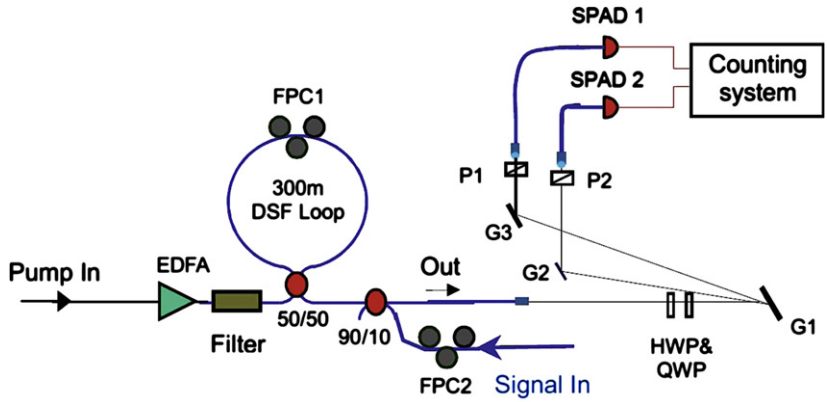

FIGURE 12.7 Schematic representation of a heralded single-photon source operating in the anomalous dispersion regime of a fiber. Pairs of photons were generated at telecoms wavelength by sFWM in a 300 m length of dispersion-shifted fiber. EDFA, erbium-doped fiber amplifier; DSF, dispersion-shifted fiber; FPC, fiber polarization controller; HWP, half-wave plate; QWP, quarter-wave plate; G, grating; P, polarizing beam-splitter; SPAD, single-photon avalanche photodiode. *Image from [33]. Copyright (year of paper) by the American Physical Society.*

can be fabricated having a short zero-dispersion wavelength, so that sFWM can be phase-matched in the 800 nm region of the spectrum (i.e., for wavelengths much shorter than the zero-dispersion wavelength of pure silica) [34,35], leading to the possibility of integration with rubidium-atom quantum memory schemes that have been proposed for the storage of entanglement. Using PCF, Sharping *et al.* demonstrated photon-pair generation using degenerate pumping at a wavelength of 749 nm, with the signal and idler photons at wavelengths of 761 and 737 nm, respectively [36]. The setup of their experiment was similar to that in Fig. 12.7 but with the DSF Sagnac-loop replaced by a straight-PCF configuration, to eliminate the complexity associated with alignment of the Sagnac interferometer in free-space. In the experiment, linearly polarized, ~ 3 ps duration pump pulses were launched into a 5.8 m section of PCF such that the plane of polarization was aligned along one of the polarization-mode axes of the fiber. For low pump powers, as the pump pulses propagated through the fiber there was a small probability that a sFWM event would occur. The resulting signal and idler photon pairs co-propagated along with the pump and emerged from the PCF. Because of such a linear configuration, efficient detection of the signal-idler pairs required aggressive filtering of the pump photons by greater than 90 dB. The resulting coincident counts and noncoincidence counts are shown in Fig. 12.8 as functions of the number of pump photons per pulse. It clearly demonstrates that more coincident photons were generated at the signal/idler wavelengths than the accidental coincidences that result from the background photons. The CAR ratio, however, is worse than that reported in

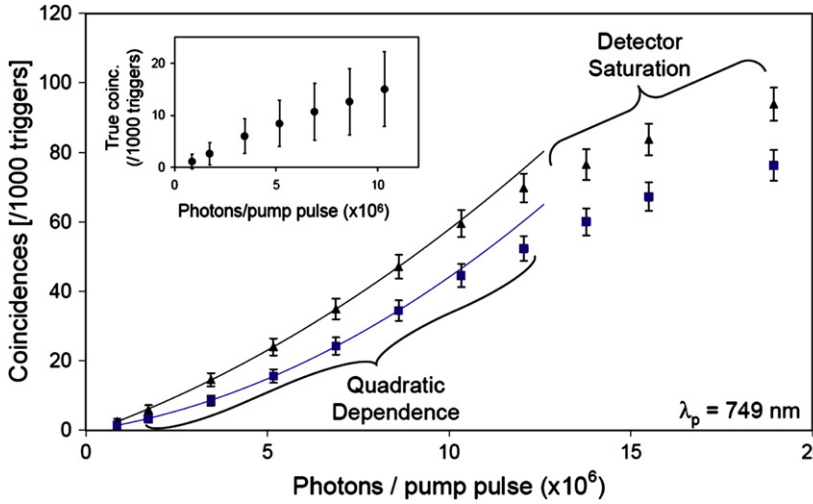

FIGURE 12.8 Plots of total coincidence counts (triangles) and accidental coincidence counts (squares) as a function of the number of pump photons per pulse with the photon counters aligned to detect at 737 and 761 nm wavelengths, respectively. At low pump powers there is a quadratic dependence of the counts on pump power, but as the power is increased the increasing signal and idler count rates start saturating the photon counters. The inset shows true coincidences (the difference between the total coincidence counts and the accidental coincidence counts) as a function of the number of pump photons per pulse. *Image from [36].*

[2,33] because the signal wavelength falls much closer to the peak of the Raman gain curve.

The above work used a degenerate pump to create nondegenerate photon pairs. Fan *et al.* demonstrated a reverse process, where two pump waves of different colors were used to create degenerate photon pairs [37]. In their experiment, linearly polarized laser pulses of 3 ps at 835 nm, output from a Ti:Sapphire oscillator operating at 80 MHz, drove the sFWM process in a 1 m section of PCF, whose output was collimated onto a high-power diffraction grating. By use of two narrow slits, a pair of linearly polarized signal (837 nm) and idler (833 nm) light pulses was selected with a FWHM bandwidth of 0.5 nm. They were then coupled into a same PCF to create degenerate photon pairs at 834.8 nm. The CAR of such photons was measured to be 8:1 with use of a 50:50 beam-splitter.

12.3.2 Photonic Crystal Fiber Sources in the Normal Dispersion Regime

The flexibility that arises from tailoring the waveguide dispersion in PCF allows the zero-dispersion wavelength (ZDW) of the fiber to be shifted to shorter wavelengths. sFWM can then be pumped at more favorable wavelengths,

typically using either picosecond pulsed, high-power fiber lasers at 1064 nm or Ti:Sapphire lasers operating around 750 nm. In both cases the PCF design can be selected to ensure that the pump laser wavelength lies in the normal dispersion region close to the zero-dispersion wavelength. The steep gradient of the phase-matching curves in this region allows the signal and idler wavelengths to be tuned over a wide range through small changes in the pump wavelength. Furthermore, the wide separation of the idler from the pump wavelength allows the idler photons to be generated far from the peak gain of the Raman-shifted pump light, significantly reducing this source of noise.

Using a PCF with a short ZDW, together with a Ti:Sapphire pump laser, means that both the signal and idler can lie within the operating range of high efficiency, silicon-based avalanche photodiodes (500–900 nm), and several such photon sources have been demonstrated to date [4,38,7,39,3]. Operating with these wavelengths can therefore allow higher potential overall efficiencies (combined optical loss and detector efficiency) than can typically be achieved when operating in the anomalous dispersion regime when both the signal and idler photons are in the near infrared range, where detector technology is less well developed. Shifting the ZDW to the shorter wavelengths required for operation in this region is achieved by increasing the size of the holes in the cladding region of the PCF, such that the air filling fraction of the cladding is higher, and by reducing the size of the core, so that the dispersion properties of the fiber approach those of narrow silica strand in air. The smaller core size relative to conventional fiber also results in a reduction in the size of the fundamental guided mode. This enhances the intensity of the guided pump light, enabling high brightness photon sources with modest pump power requirements.

Fulconis *et al.* [3] demonstrated a source of photon pairs at 587 and 897 nm, pumped using 4 ps pulses from a Ti:Sapphire laser at 708 nm. A PCF with a core diameter of 2 μm, shown in Fig. 12.9, was used to shift the ZDW of the fiber to 715 nm, as required to achieve phase-matching. Due to the high pump intensity resulting from the small mode field diameter of the fiber, a high brightness of 3.2×10^5 s^{-1} detected photon pairs was achieved with an average pump power of 540 μW (1.8 kW peak power), giving a spectral brightness of 4×10^5 s^{-1} mW^{-2} nm^{-1} for the heralded signal photons (see Fig. 12.10). Fan *et al.* [38] demonstrated a heralded photon source based on a similar PCF structure, generating signal and idler photons at 690.4 and 801.2 nm using a 742 nm pump. A detected pair brightness of 9×10^4 s^{-1} mW^{-2} nm^{-1} was achieved for a CAR near 10. A maximum CAR of 900 was measured for the source at low pump power, but the resulting detected pair brightness was reduced to just 45 s^{-1}. For both of these sources, the overall transmission efficiencies for the signal and idler arms were $\sim$ 15%, with the implemented free-space spectral filtering and the coupling efficiency into standard single-mode fiber accounting for the majority of the loss.

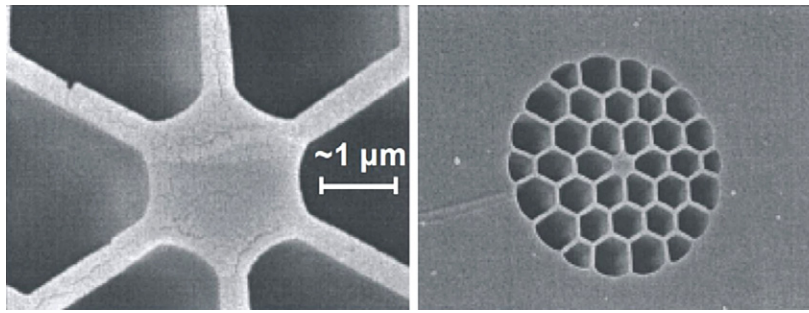

FIGURE 12.9 Scanning electron microscope images showing the cross-section of a highly nonlinear PCF. *Images from [3].*

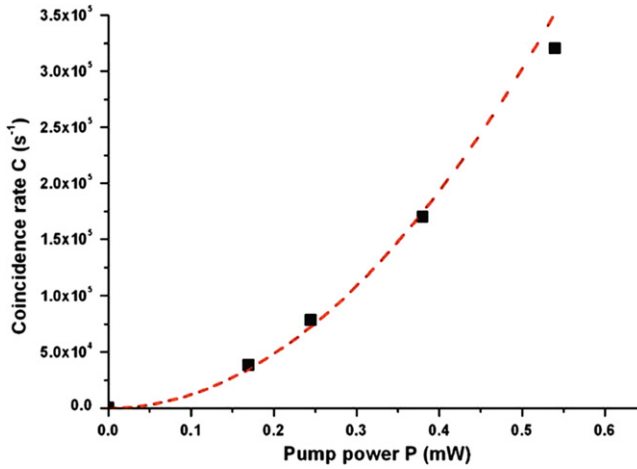

FIGURE 12.10 Measured twofold coincidence count rate as function of average pump power for the photon source described in [3]. *Image from [3].*

Another interesting approach, with alternative applications, is to generate widely spaced signal and idler photons, with the signal near 800 nm and the corresponding idler photons in the telecommunications band near 1550 nm [1,5,40]. Photons at the idler wavelength can then be transmitted over long distances in optical fibers with minimal loss. At the same time, the wavelength of the signal photons makes them well suited for interfacing with quantum memories, or for processing using quantum logic gates (see Section 12.7), due to the high detection efficiency. This type of source is therefore of considerable interest for many quantum communications applications, such as quantum repeaters [41]. Photon pairs at these wavelengths can be generated using a pump wavelength of 1064 nm, with phase-matching satisfied in the normal dispersion regime of a suitably designed PCF with a ZDW near 1090 nm.

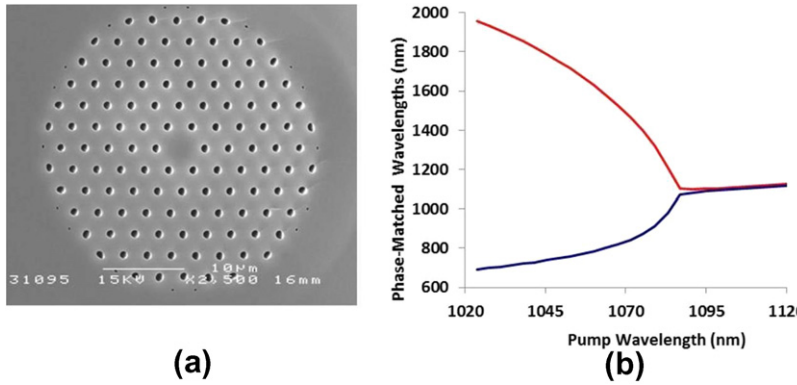

FIGURE 12.11 (a) Scanning electron microscope image of a PCF used to generate signal and idler pairs, widely spaced in frequency as described in [5] and (b) the associated calculated phase-matching curve. *Images from [5].*

The PCF structure required for phase-matching in this type of source has a larger core diameter and lower air filling fraction than for Ti:Sapphire pumped sFWM, as the desired dispersion profile is closer to that of the intrinsic material dispersion. Due to the weaker confinement of the guided mode, and the inherently lower efficiency of sFWM when operating at longer wavelengths, the pump power requirements are typically higher for this type of source. However, the larger core size does allow the PCF to be more easily integrated with conventional single-mode fibers, due to the similarity in mode field profile. Techniques for splicing PCF structures of this type to single-mode fiber have been demonstrated with losses < 1 dB [42]. The lower air filling fraction and larger core also mean that this type of PCF can exhibit endlessly single-mode guidance [43], further improving the compatibility with conventional fibers. McMillan *et al.* [5] demonstrated an all-fiber heralded photon source based on a PCF design of this type (see Fig. 12.11). A picosecond-pulsed pump at 1064 nm generated signal and idler pairs at 802 and 1570 nm respectively. By using low loss, spliced telecom components to separate and spectrally filter the photons, a transmission efficiency of 68% was demonstrated at the idler wavelength, giving a heralding efficiency of 52%.

12.4 QUANTUM INTERFERENCE BETWEEN SEPARATE SPECTRALLY FILTERED FIBER SOURCES

One striking result of the nonclassical nature of single-photon states is the observation of two-photon quantum interference that can occur when two single photons are incident on the two input ports of a beam-splitter. For a 50:50 beam-splitter, when the two input photon states are both pure and indistinguishable the

photons will bunch and both exit from the same output port of the beam-splitter, an effect known as Hong-Ou-Mandel (HOM) interference [44] as introduced in Chapter 2. As the HOM effect can be used to implement an effective two-photon interaction, it performs a critical role in many quantum information applications, including quantum logic gates based on the model of linear optical quantum computation (see Section 12.7), and the generation of large entangled cluster states through photonic fusion (see Section 12.8). Achieving high visibility HOM interference between photons from independent fiber-based photon sources is an essential requirement for demonstrating their suitability for use in such applications, and it also serves as a convenient approach for measuring the purity of the photon states generated by such sources.

A general beam-splitter, with reflection and transmission coefficients r and t, can be described by transformation relations between its input modes a_1 and a_2 and output modes b_1 and b_2 in terms of photon creation operators by

$$\hat{a}_1^\dagger = r\hat{b}_1^\dagger + t\hat{b}_2^\dagger, \tag{12.15}$$

and

$$\hat{a}_2^\dagger = t\hat{b}_1^\dagger - r\hat{b}_2^\dagger, \tag{12.16}$$

where the phase-shift seen for the reflected term in Eq. (12.16) is required to satisfy conservation of energy [45]. For an input state of the form $\hat{a}_1^\dagger\hat{a}_2^\dagger|vac\rangle$, where two indistinguishable single-photon states are input, one into each arm of the beam-splitter, the output state after the beam-splitter is given by

$$\begin{aligned} |\psi_{out}\rangle &= (r\hat{b}_1^\dagger + t\hat{b}_2^\dagger)(t\hat{b}_1^\dagger - r\hat{b}_2^\dagger)|vac\rangle \\ &= (rt\hat{b}_1^\dagger\hat{b}_1^\dagger + (t^2 - r^2)\hat{b}_1^\dagger\hat{b}_2^\dagger - rt\hat{b}_2^\dagger\hat{b}_2^\dagger)|vac\rangle. \end{aligned} \tag{12.17}$$

In the case of a 50:50 beam-splitter, $r = t = \frac{1}{\sqrt{2}}$, and the output state of the system is given by

$$|\psi_{out}\rangle = \frac{1}{2}(\hat{b}_1^\dagger\hat{b}_1^\dagger - \hat{b}_2^\dagger\hat{b}_2^\dagger)|vac\rangle = \frac{|2\rangle_{b1}|0\rangle_{b2} - |0\rangle_{b1}|2\rangle_{b2}}{\sqrt{2}}. \tag{12.18}$$

Showing that both photons will emerge from the same output of the beam-splitter (either b_1 or b_2). The cancellation of the $\hat{b}_1^\dagger\hat{b}_2^\dagger$ terms in Eq. (12.17) relies on the output photon modes being indistinguishable, so that the reflected and transmitted terms are equivalent. If the single photons which are input are distinguishable from each other in any degree of freedom then they will not interfere, and will behave like classical particles with each being either transmitted or reflected with 50% probability. HOM interference between single photons can be demonstrated, for example, by introducing a variable delay to the arrival time of one of the photons at the beam-splitter, such that at zero delay the photons are indistinguishable, but at delays greater than their coherence length they are entirely distinguishable.

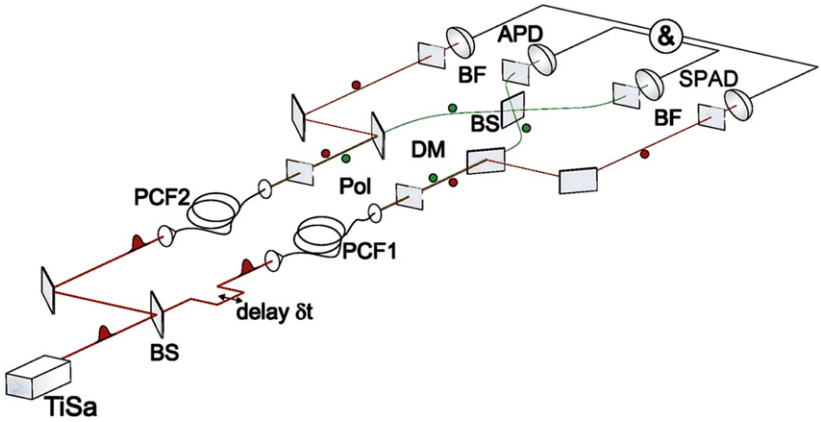

FIGURE 12.12 Experimental setup used to demonstrate HOM interference between two heralded single-photon sources. A time delay δt is incorporated in one of the sources using a retroreflector, to adjust the relative arrival time of the interfering photons at the central beam-splitter. BS, beam-splitter; DM, dichroic mirror; BF, spectral band-pass filter; pol, polarizer; SPAD, single-photon avalanche photodiode. *Image from [10].*

Figure 12.12 shows a typical experimental setup used to demonstrate HOM interference between two fiber-based pair-photon sources. At the output of the section of nonlinear fiber in each source, the generated photons are separated by wavelength, and one photon of the pair (in this case the idler photon) is detected and used to herald the presence of the other. The heralded single photons are overlapped at a beam-splitter and the coincident counts between the detectors are measured as the variable time delay to the pump pulses for one of the sources is varied. The interference is observed as a dip in the fourfold coincidence count rate between the two heralding and two interfering photons when the signal photons from the two sources are overlapped at the beam-splitter.

The visibility of the interference feature is dependent on the purity of the single-photon states that are generated, and will be reduced by the presence of additional, noninterfering noise photons. If two independent sources are used to generate heralded single photons, then the degree to which the properties of the interfering photons are matched will also influence the interference visibility. For single-photon states to be considered indistinguishable, they must be identical in all degrees of freedom. This includes their spectral properties, temporal mode (relative output time from the source), spatial mode, and polarization state.

Ensuring that the interfering photons are in matching spatial modes can be easily achieved in fiber-based sources, as fibers can be designed such that only a single spatial mode is supported at the desired single-photon wavelength. These sources can also be coupled with low loss to single-mode fused-fiber couplers, which perform an identical operation to free-space beam-splitters, allowing

the HOM interaction to take place in an all-fiber configuration. Photons can also readily be generated in a well-defined polarization state in optical fibers by making use of fibers with birefringence. In a birefringent fiber, if linearly polarized laser pump light is launched onto one of the principal fiber axes, its polarization state will be preserved along the fiber length. If the birefringence is sufficiently strong, it will also modify the phase-matching conditions for sFWM, such that the generation of photons at the selected wavelength can only occur on one axis of the fiber. Matching of the polarization state of photons produced from independent sources can be achieved using standard wave plates in a free-space implementation, or with fiber polarization controllers if the photons are delivered in single-mode fiber.

The requirements to realize a heralded photon in a single temporal mode are intimately related to the spectral properties of the state. The coherence time of a generated photon will be determined either by the gain bandwidth of the sFWM process itself, or by the bandwidth of any spectral filtering that has subsequently been applied if this is narrower than the initial unfiltered state. For a photon wave-packet with a Gaussian spectral profile, central wavelength λ_0, and full-width half-maximum bandwidth $\Delta\lambda$, the coherence time τ_{coh} is given by

$$\tau_{\text{coh}} = \frac{2\ln 2}{\pi n c}\frac{\lambda_0^2}{\Delta\lambda}, \tag{12.19}$$

where n is the refractive index of the transmission medium and c is the speed of light in free-space. For a photon source driven by a pulsed pump, the coherence time of the photons should be longer than the pump pulse duration, so that only a single temporal mode is available for the photon pair to be generated in within the timing gate defined by the pump pulse. In that case the desired single-photon state will be pure upon heralding. If the coherence time of the photon is shorter, then due to the limited timing resolution of current realistic photon detectors, the detection of a heralding photon will project its partner into a mixed state.

To meet the required photon coherence time for purity, the heralded photon is often spectrally filtered. For sources pumped with femtosecond laser pulses, the required filtering bandwidth is a few nanometers, which can be readily implemented using standard interference filters. On the other hand, for picosecond pulsed sources the heralded photons may need to be filtered to a bandwidth ~0.1 nm, which is more challenging to achieve with low loss. For an experimental setup of the type shown in Fig. 12.12, the maximum visibility of the HOM interference when the photons are overlapped at the beam-splitter is given by [46]

$$V_{\text{max}} = \frac{\sqrt{1+\sigma^2/\sigma_{\text{p}}^2}}{1+\sigma^2/2\sigma_{\text{p}}^2}, \tag{12.20}$$

where the signal and idler photons are assumed to be filtered using energy-matched, Gaussian profile spectral filters of bandwidth σ, defined by the filtering

function

$$f_j(\omega_j) = \frac{1}{N} e^{(\omega_{j0}-\omega_j)^2/\sigma^2}, \tag{12.21}$$

where $j = s,i$ denotes the signal or idler, ω_{j0} is the central frequency of the filter and N is a normalizing constant. Similarly, the pump pulse is assumed to be a Gaussian pulse of bandwidth σ_p. As shown in Fig. 12.13, although the maximum interference visibility reaches unity only in the limit when the bandwidth of the spectral filtering ratio tends to zero, visibility of 90% or more is achieved for filtering bandwidths only slightly less than that of the pump bandwidth.

It should be noted that this analysis neglects the effect of group velocity walk-off between the pump and the generated signal and idler, which becomes relevant when dealing with short-duration pump pulses. For the sFWM process described in Section 12.2, phase-matching can be satisfied with the pump close to the ZDW, which coincides with a local minimum in the group velocity of the fiber. For widely separated signal and idler wavelengths the dispersion of the fiber can lead to a significant mismatch between the group velocities of the generated photons with the pump. Pulse walk-off limits the minimum bandwidth of the signal and idler that will be generated and the sFWM gain grows only linearly with the fiber length in this regime. More importantly, walk-off can broaden the emission time of the photon pair beyond the single temporal mode defined by the coherence time of the filtered photon. The walk-off effect is manifested as a timing jitter in the output time of the photons relative to the laser pulses, and the fiber length must be chosen such that this jitter is small in comparison to the coherence length. For photon sources operating in the anomalous dispersion regime of a fiber (see Section 12.3.1), where the generated

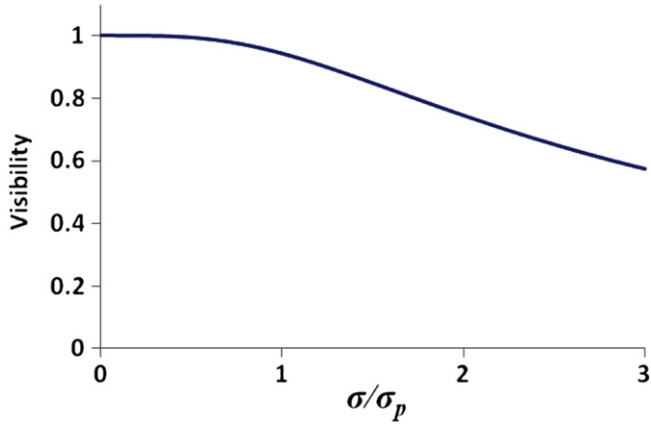

FIGURE 12.13 Theoretical maximum visibility for HOM interference as a function of the spectral filtering bandwidth σ relative to the pump pulse bandwidth σ_p, given by Eq. (12.20). *Image from [32].*

photons may be separated by only tens of nanometers, the limit to the maximum fiber length may be hundreds of meters, while for sources with widely separated signal and idler wavelengths (see Section 12.3.2) the limit can be as little as a few centimeters.

Interference between spectrally filtered photons, generated independently in two separate sections of identical PCF (pumped using the same laser), has been demonstrated with visibility greater than 90% (see Fig. 12.14)) [46]. When operating such sources with low brightness, this interference can be observed in the raw fourfold count rates of the detectors. When the brightness of the source is increased toward 0.1 generated pairs per pulse, the raw visibility is reduced due to the presence of multiple pair generation events in each source, which do not interfere fully. When the average number of pairs per pulse $\overline{n}$ is low, and distinguishability in other degrees of freedom is negligible, the visibility is given by

$$V_{\max} \approx \frac{1 + 8\overline{n}}{1 + 12\overline{n}}. \tag{12.22}$$

The visibility of interference between the sources in the absence of multiple pairs can be determined by measuring the background fourfold count rates due to each source individually, and subtracting these background terms in order to find the net visibility. While the presence of this background term is undesirable for practical applications, measuring the net visibility of interference with higher pump power can be useful for demonstrating the purity of the generated single-photon states. In the future, post-selection using photon-number resolving detectors will allow the contribution from these higher photon-number states to removed.

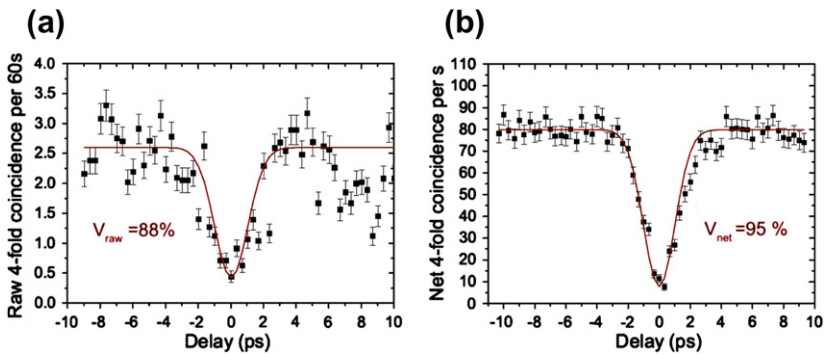

FIGURE 12.14 Experimental demonstration of quantum interference between photons output from separate PCF sources, seen as a dip in the measured fourfold coincidence count rate of signal and idler photons from the two sources (a) with 1 mW average pump power and (b) with 8 mW average pump power and corrected for background from multiphoton emission. *Images from [46].*

12.5 INTRINSICALLY PURE-STATE PHOTONS

12.5.1 Generation of Spectrally Uncorrelated Two-Photon States Through Group Velocity Matching

As described in Section 12.4, achieving high visibility quantum interference between independent heralded photon sources requires that the heralded photons be prepared in pure and indistinguishable states. When generating photon pairs through sFWM, the bandwidth of the gain of the process typically allows some variation in the signal and idler wavelengths. This is due to both the finite pump bandwidth, which is necessarily broadened in short pulse duration laser sources, and because of the possibility of generating pairs which are not perfectly phase-matched in a realistic fiber of finite length. Considering only the spectral degree of freedom, the two-photon state generated by sFWM with degenerate pumping can be expressed in the form

$$|\Psi\rangle \propto \iint d\omega_s d\omega_i F(\omega_s,\omega_i)\hat{a}_s^\dagger(\omega_s)\hat{a}_i^\dagger(\omega_i)|vac\rangle, \tag{12.23}$$

where $\hat{a}_{s,i}^\dagger(\omega_{s,i})$ are the photon creation operators for signal and idler photons at frequencies ω_s and ω_i respectively, and $|vac\rangle$ is the vacuum state. $F(\omega_s,\omega_i)$ is the joint spectral amplitude function (JSA), which is dependent on both the pump amplitude profile $\alpha(\omega_s+\omega_i)$ and the phase-matching function $\phi(\omega_s,\omega_i)$, with

$$F(\omega_s,\omega_i) = \alpha(\omega_s+\omega_i)\phi(\omega_s,\omega_i). \tag{12.24}$$

The function $\alpha(\omega_s+\omega_i)$ describes the variation in the signal and idler frequencies that are possible due to the finite bandwidth of the pump pulse. The pump is commonly assumed to be Gaussian in profile so that

$$\alpha(\omega_s+\omega_i) = \exp\left(-\frac{(\Delta\omega_s+\Delta\omega_i)^2\sigma^2}{2}\right), \tag{12.25}$$

where $\Delta\omega_j = \omega_j - \omega_{j0}$ are the detunings of the signal and idler frequencies ω_j away from their peak values ω_{j0}, and σ is related to the full-width half-maximum frequency bandwidth of the pump pulse $\Delta\omega_p$ by $\sigma = 2\sqrt{\ln 4}/\Delta\omega_p$. The phase-matching function is given by [8,10]

$$\phi(\omega_s,\omega_i) = \exp\left(\frac{i\kappa L}{2}\right)\mathrm{sinc}\left(\frac{\kappa L}{2}\right) \tag{12.26}$$

for a fiber of length L, where κ is the phase-mismatch defined in Eq. (12.3).

The JSA is dependent on both the signal and idler frequencies. Because of this the energy and phase-matching requirements generally impose strong correlations in their spectra. When one photon of the pair is detected as a herald, information can in principle be extracted about the state of the other photon. However, since realistic single-photon detectors are unable to resolve

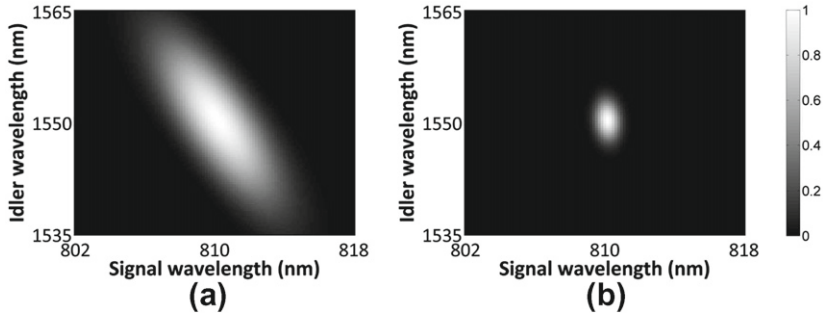

FIGURE 12.15 (a) JSA plot showing correlation between the idler and signal wavelengths and (b) appropriate narrowband spectral filtering can be applied in order to reduce the correlation. *Image from [32].*

which spectral mode the heralding photon is in, this information is not generally experimentally accessible to the observer of the system with standard single-photon detectors. This projects the heralded single photon into a mixed state, which is a statistical mixture of the available pure states [47].

Figure 12.15a shows the JSA of the two-photon state generated by a typical PCF structure (similar to that shown in Fig. 12.11 used for generating widely separated signal and idler photons pumping in the normal dispersion regime). The undesirable frequency correlation is clearly apparent. As described in Section 12.4, narrowband spectral filtering can be implemented to approximate a single spectral mode, such that a pure heralded single-photon state can be realized, which is the approach taken by all of the photon sources outlined in Sections 12.3.1 and 12.3.2. The effect of spectral filtering can be incorporated into Eq. (12.23) by multiplying the JSA function of the photon pair generated by the fiber by functions $f_s(\omega_s)$ and $f_i(\omega_i)$, describing the spectral profile of the filtering applied to the signal and idler respectively. This reshapes the JSA, and for sufficiently narrowband filtering the correlation between the signal and idler wavelengths is reduced, as demonstrated in Fig. 12.15b. However, implementing narrowband spectral filtering usually introduces significant loss, which reduces both the source brightness and heralding efficiency. This is particularly significant in quantum information experiments involving higher photon numbers, in which multiple heralded photon sources are required to operate simultaneously in order to generate an N-photon state. If the probability of detection of each individual photon is μ, the overall probability of generating the required N-photon state is given by μ^n. This typically limits N to $\sim$6 before the measured count rates for experiments become prohibitively low. Additionally, narrowband filtering leads to the majority of the photon pairs generated by sFWM being discarded, significantly increasing the pump power required to achieve the desired source brightness within the operating spectral bandwidth.

An alternative approach to narrowband spectral filtering is to design fiber with a dispersion profile that minimizes the correlation between the generated signal and idler frequencies, and hence allows pure states to be heralded without the need for filtering [8]. From Eq. (12.23) it can be shown that the correlation between the signal and idler photon wavelengths will be eliminated if the JSA function can be factorized such that $F(\omega_s,\omega_i) = F_s(\omega_s)F_i(\omega_i)$, so that the two-photon state can be written as a product of the signal photon state and idler photon state as [48]

$$|\Psi\rangle \propto \left(\int d\omega_s F_s(\omega_s)\hat{a}_s^\dagger(\omega_s)\right) \times \left(\int d\omega_i F_i(\omega_i)\hat{a}_i^\dagger(\omega_i)\right)|vac\rangle. \quad (12.27)$$

The contribution to the correlation in the JSA from the pump amplitude function $\alpha(\omega_s + \omega_i)$ is due to energy conservation, and the shape of this function always forms an angle of $-45°$ to the signal frequency axis of the JSA plot, with the width of the function determined by the bandwidth of the pump pulse. In contrast, the angle of the phase-matching function on the JSA plot can be rotated by tailoring the dispersion properties of the fiber. By using a linear approximation to the phase-mismatch κ, around the signal and idler frequencies where perfect phase-matching is achieved, the angle of the phase-matching function relative to the signal frequency axis on the JSA plot is found to be [8]

$$\theta_{pm} = -\arctan\left(\frac{\delta_s}{\delta_i}\right), \quad (12.28)$$

with

$$\delta_j = L\left(\left.\frac{dk_p}{d\omega}\right|_{\omega_{p0}} - \left.\frac{dk_j}{d\omega}\right|_{\omega_{j0}}\right) = L\left(\frac{1}{v_p} - \frac{1}{v_j}\right), \quad (12.29)$$

where $j = s, i$ and v_s, v_i and v_p are the group velocities of the signal, idler, and pump.

The form of Eq. (12.28) suggests two possible strategies for generating spectrally uncorrelated two-photon states. In the first, the group velocity of the pump is chosen to lie exactly halfway between those of the signal and idler, which is known as symmetric group velocity matching. The second possible approach, asymmetric group velocity matching, involves matching the group velocity of either the signal or idler field to that of the pump. Both symmetric and asymmetric group velocity matching have been demonstrated using cross-polarized sFWM in birefringent fibers, where the additional flexibility provided by the birefringence enables the group velocity of the pump field on one axis of the fiber to be shifted relative to the group velocity of the generated photon wavelengths on the other axis.

Factorable two-photon states generated by symmetric group velocity have been demonstrated using birefringent PCF [49] and highly birefringent conventional fibers [9,11]. Selecting a fiber with an appropriate birefringence,

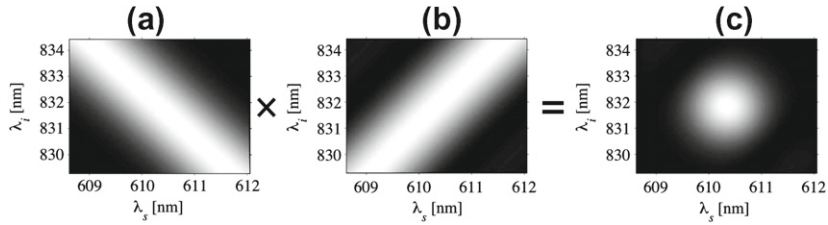

FIGURE 12.16 JSA for symmetric group velocity matching technique. (a) Pump amplitude function; (b) phase-matching function forming an angle of 45° to the signal axis; and (c) resulting JSA with symmetric signal and idler frequency distribution. *Images from [9].*

where the signal and idler group velocities lie on either side of the pump, sets $\theta_{pm} = +45°$. Then, for a given pump bandwidth, the length of the fiber can be selected so that the contribution to the two-photon correlation from the phase-matching function will counteract the correlation due to the pump amplitude function, as shown in Fig. 12.16. Smith *et al.* demonstrated the generation of spectrally uncorrelated signal and idler states of this type at 610 and 830 nm using a 10 cm length of commercial birefringent fiber pumped with femtosecond pulses from a Ti:Sapphire laser at 704 nm, achieving a measured brightness of 100 pairs $s^{-1}mW^{-2}$ [9].

In the case of asymmetric group velocity matching, designing the fiber so that either the signal or idler velocity is matched to that of the pump leads to the phase-matching function being oriented horizontally or vertically respectively on the JSA plot ($\theta_{pm} = 0°$ or 90°). These conditions are found to coincide with positions on the phase-matching plot where the gradient of either the signal or idler wavelength generated becomes zero with respect to changes in the pump field wavelength. At these points, as long as the bandwidth of the phase-matching function is sufficiently narrow compared to that of the pump amplitude function, the overall two-photon state becomes uncorrelated, although the frequency bandwidths of the signal and idler are not identical in this case. The photon which propagates with same group velocity as the pump is well localized in time, so its partner photon carries all of the timing uncertainty of the pair. As a consequence of the joint energy-time uncertainty of the photon pair, the photon which walks-off in time from the pump pulse exhibits a naturally narrow bandwidth, as shown in Fig. 12.17.

Halder *et al.* [10] demonstrated a heralded single-photon source generating naturally narrowband signal photons at 597 nm by pumping a 40 cm section of birefringent PCF with 0.8 ps pulses at 705 nm from a Ti:Sapphire laser. The measured signal photon bandwidth of 0.13 nm was greatly reduced compared to the bandwidth (∼3 nm) of unfiltered photons generated by sFWM in previous experiments with comparable operating wavelengths [3]. HOM interference was measured between the signal photons generated by two independent, identically prepared sources based on this fiber, showing a raw visibility of 76%.

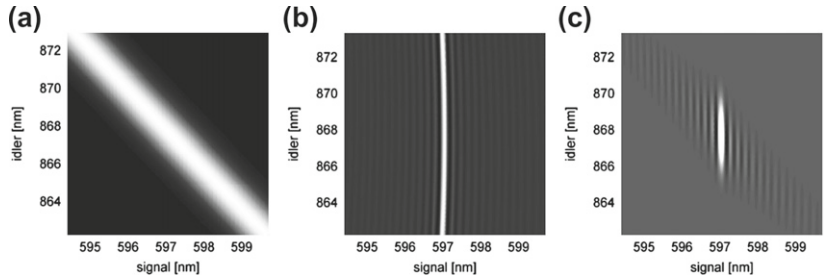

FIGURE 12.17 JSA for the PCF described in [10], designed to generate naturally narrowband signal photons through asymmetric group velocity matching. (a) Envelope of the pump intensity, (b) phase-matching condition of the PCF, and (c) JSA of the created photon pair. *Image from [10].*

In contrast to spectrally filtered photon sources based on co-polarized sFWM, the visibility of HOM interference is expected to be higher when using a longer fiber length [50]. This means that the brightness and purity of the source could both be improved, indefinitely in principle, by increasing the fiber length. In reality, current limitations in the fiber manufacturing process lead to fluctuations in the fiber structure (and consequently the phase-matching conditions) which typically limit the maximum length to < 1 m.

As with spectrally filtered sources, widely spaced photon-pair generation with the idler wavelength in the telecoms band near 1550 nm is of considerable interest. The generation of naturally narrowband idler photons at 1550 nm has been demonstrated using a 1064 nm picosecond-pulsed pump source operating in the anomalous dispersion regime of a highly birefringent PCF [51]. For PCF with sufficiently strong waveguide dispersion, a second ZDW can be shifted into the transparency window of the fiber in the near infrared, also allowing a factorable two-photon state to be generated by co-polarized sFWM without the need for birefringent phase-matching. This is made possible by the fact the phase-matching curves form closed loops, with turning points on the outer edges of the loops where either the signal or idler become narrowband [8]. This was exploited by Söller *et al.* to generate widely separated, spectrally factorable signal and idler photons at 514 and 1542 nm from a 771 nm pump source [6].

12.5.2 A Temporal Filtering Approach for Attaining Pure-State Photons

As shown in Section 12.4, applying narrowband spectral filtering to the photon states produced by sFWM can provide a close approximation to a spectrally pure heralded single-photon source, allowing high visibility HOM interference to be achieved. One drawback with the use of narrowband spectral filtering, however, is that the production rate of the heralded photons is low because most usable pairs are filtered out. This problem can not be overcome by simply increasing the pump power in the photon-pair source, since doing so will lead

to strong background noise arising from multipair emission. Section 12.5.1 outlined one possible solution to this dilemma—a proposal by Grice *et al.* [48], who suggested creating the photon pairs in spectrally factorable states so that measuring the signal photon would not disclose any spectral information about the idler. Since the narrowband filters are not needed, this approach can dramatically improve the single-photon production rate. With such motivation, extensive efforts have been made to study the creation of spectrally factorable photon pairs [52,53] and a few experimental demonstrations have been made [54–57]. However, progress has been limited due to the practical difficulty of simultaneously achieving appropriate phase-matching and group velocity matching. More importantly, one has to wait for a relatively long time before a second short-duration photon can be heralded, as in this case the signal (or equivalently the idler) photon must have a bandwidth much narrower than the pump to achieve the spectral factorability. Due to this, the repetition rate of the heralded single-photon creation is restricted, resulting in a relatively low production rate.

To overcome the aforementioned limitations, Huang *et al.* proposed an approach that does not rely on narrow spectral filtering or spectral factorability of the photon pairs [58]. It is based on time and bandwidth limited detection of the signal photons in a single-mode regime [59], achieved by using a broadband filter and an on/off detector whose measurement window is shorter than the coherence time of the signal photons. To understand the principle of single-mode detection, consider amplitude profiles $f(t)$ and $h(\omega)$ for the time gate and the sequential spectral filter, respectively. The number operator for output photons is given by $\hat{n} = \frac{1}{(2\pi)^2}\int d\omega d\omega' \kappa(\omega,\omega')\hat{a}^\dagger(\omega)\hat{a}(\omega')$ [59,60], where $\hat{a}(\omega)$ is the annihilation operator for the incident photons of angular frequency ω, satisfying

$$[\hat{a}(\omega), \hat{a}^\dagger(\omega')] = 2\pi\delta(\omega - \omega'). \tag{12.30}$$

$$\kappa(\omega,\omega') = \int dt\, h^*(\omega)h(\omega')|f(t)|^2 e^{i(\omega-\omega')t} \tag{12.31}$$

is a Hermitian spectral correlation function, which can be decomposed onto a set of Schmidt modes as

$$\kappa(\omega,\omega') = \sum_{j=0}^{\infty} \chi_j \phi_j^*(\omega)\phi_j(\omega'), \tag{12.32}$$

where $\{\phi_j(\omega)\}$ are the mode functions satisfying

$$\int d\omega \phi_j^*(\omega)\phi_k(\omega) = 2\pi\delta_{j,k} \tag{12.33}$$

and $\{\chi_j\}$ are the decomposition coefficients satisfying $1 \geq \chi_0 > \chi_1 > \cdots \geq 0$. Introducing an infinite set of mode operators via ($j = 0,1,\ldots$)

$$\hat{c}_j = \frac{1}{2\pi}\int d\omega \hat{a}(\omega)\phi_j(\omega) \tag{12.34}$$

that satisfy $[\hat{c}_j, \hat{c}_k^\dagger] = \delta_{jk}$, the output photon-number operator for the filtering device can be rewritten as

$$\hat{n} = \sum_{j=0}^{\infty} \chi_j \hat{c}_j^\dagger \hat{c}_j. \tag{12.35}$$

This result indicates that $\{\phi_j(\omega)\}$ have an intuitive physical interpretation: as "eigenmodes" with eigenvalues $\{\chi_j\}$ of the filtering device. In this physical model, the filtering device projects incident photons onto the eigenmodes, each of which are passed with a probability given by the eigenvalues. Specifically, for $\chi_0 \sim 1$ and $\chi_{j\neq 0} \ll 1$ (achievable with an appropriate choice of spectral and temporal filters, as shown below) only the fundamental mode is transmitted while all the other modes are rejected. In this way, truly *single-mode* filtering can be achieved. When combined with a single-photon detector, this can be extended to a single-mode, single-photon detection system. Regardless of the type of spectral and temporal filters used to achieve this kind of single-mode filtering, such a system is capable of separating photons which, even though they may exist in the same spectral band and the same time bin, have different mode structures.

Figure 12.18a shows example plots of χ_0, χ_1, and χ_2 as functions of $c \equiv BT/4$ for a rectangular-shaped spectral filter with bandwidth B and a rectangular-shaped time window of duration T [59,61]. For $c < 1, \chi_0 \approx 1$ is obtained with $\chi_1, \chi_2 \ll 1$, giving rise to approximately single-mode filtering. Note that this behavior is true for any B, as long as $T < 4/B$. In other words, $\{\chi_j\}$ depend only on the product of B and T, rather than on their specific values. Consequently, even a broadband filter can lead to a single-mode measurement over a sufficiently short detection window, and vice-versa. To understand this, consider the case where a detection event announces the arrival of a signal

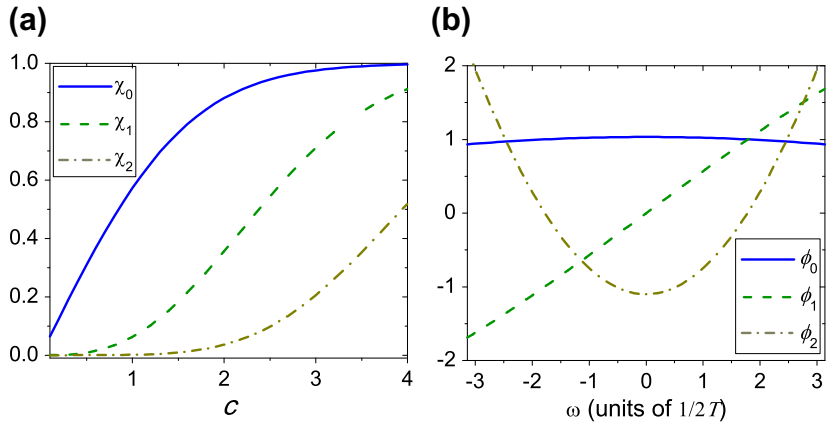

FIGURE 12.18 (a) χ_0, χ_1, and χ_2 as functions of c. (b) Plots of ϕ_0, ϕ_1, and ϕ_2 for $B = \pi/T$ (corresponding to $c = \pi/4$). *Images from [58]. Copyright (year of paper) by the American Physical Society.*

photon at an unknown time within the window T. In the Fourier domain, this corresponds to a detection resolution of $1/T$ in frequency. Given $c < 1$ or $1/T > B/4$, the detector is thus unable to, even in principle, reveal the frequency of the signal photon. Therefore, the signal photon is projected onto a quantum state in a coherent superposition of frequencies within B [62]. This can be seen in Fig. 12.18b, where the fundamental detection mode has a nearly flat profile over the filter band $[-B/2, B/2]$. Lastly, since $T < 4/B$ is required, the pass probability of the fundamental mode will be subunity, but not significantly less than one.

By using single-mode detection, even nonfactorable states can also lead to high-purity heralded single photons without the use of narrowband filters. By using multimode theory to take into account the effect of multiple photon-pair emission, distinctly superior heralding performance was achieved relative to those obtainable via narrow spectral filtering alone or tailoring the phase-matching properties of nonlinear media to obtain spectrally factorable photon-pair states [62]. The theory can also be used to numerically optimize the spectral and temporal filter widths for a variety of photon-pair correlations. The results reveal that while the optimization conditions vary for different correlations, the final performance using optimized filters is always quite similar. This interesting phenomenon suggests that the key to achieving high performance in the heralded creation of single photons is to apply an appropriate measurement scheme to the signal photons [62].

The above theory was validated by a heralded two-photon interference experiment in an all-fiber setup in both multimode ($c > 1$) and single-mode ($c < 1$) regimes [12]. In the experiment, pairs of signal and idler photons were generated in two separate optical fiber spools via sFWM driven by pulsed pumps. By detecting the idler photons created in each spool, the generation of their partner (signal) photons was heralded. To quantify their indistinguishability, the signal photons generated separately from the two spools were mixed on a 50:50 beam-splitter and HOM interference measurements were performed. By changing effective T for the idler photons, heralded generation of single photons in the multimode and single-mode regimes can be realized. The experimental results are shown in Fig. 12.19, where the HOM visibility was found to be quite low (19(2)%) when the signal photons have a temporal length $T > 1/B$ ($c = 3.8$ in this case), owing to the presence of photons with many distinguishable degrees of freedom. However, when $T < 1/B$ ($c = 0.7$ in this case), for which a single-mode detection is effectively realized, a much higher HOM visibility (72(7)%) is obtained. In all cases, the experimental data are in good agreement with predictions of the above multimode-detection theory with careful modeling of multi-pair production, Raman emission, loss, dark-count noise, and the interference between the two arms of a real experimental system, without the need for any fitting parameter. This experiment highlights the single-mode filtering as a viable tool for erasing the quantum distinguishability of single photons.

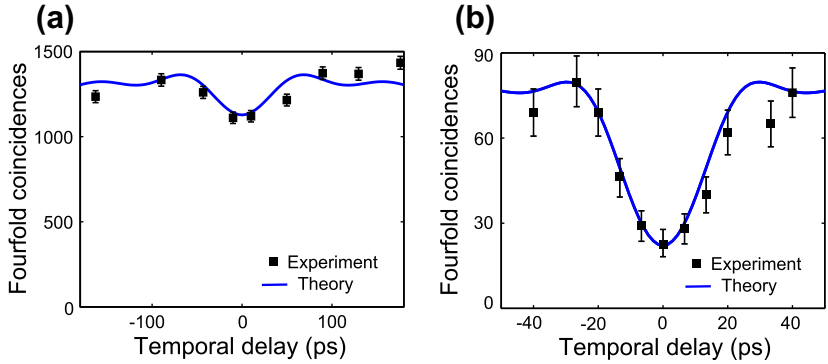

FIGURE 12.19 (a) Fourfold coincidence counts per 20 billion pump pulses recorded as a function of the relative delay between signal photons in the multimode configuration and (b) fourfold coincidence counts per 10 billion pump pulses recorded as a function of the relative delay in the single-mode configuration. In both plots, the error bars are computed following the standard procedure of estimating statistical fluctuations assuming Poisson distributions for the recorded coincidence and single counts. See text for more details on the theory curves in both plots which are overlaid without the use of any fitting parameter. *Images from [12]. Copyright (year of paper) by the American Physical Society.*

12.6 ENTANGLED PHOTON-PAIR SOURCES

The concept of entanglement, in which the quantum states of two or more physically separate systems may be linked, is one of the defining characteristics of quantum mechanics. The pioneering early work of Aspect *et al.* on the nature of entangled photon pairs demonstrated that the state of one photon could not be described independently of the state of the other, meaning that a measurement made on one member of the pair can instantaneously affect the state of its partner [63]. In recent years, efficient, high-fidelity sources of entangled photons have become an essential resource for many quantum information applications, including quantum cryptography and communications protocols [64–66], quantum repeaters [67], quantum memories [68], and schemes for quantum computation [69–71]. An optical fiber-based source of entangled photons can be realized by preparing signal and idler photon pairs through sFWM in such a way that the states of the two photons are correlated in one or more of their degrees of freedom. For many applications, polarization-entangled photons are particularly useful, as the polarization state of light can be easily manipulated and measured using standard linear optical components such as wave plates and polarizers.

The Sagnac-loop configuration shown in Fig. 12.20 can be used to generate entangled photon pairs from a fiber through a counterpropagating scheme [14]. In this scheme, a loop of nonlinear fiber, capable of producing pairs of signal and idler photons by sFWM (as detailed in Section 12.2), is pumped simultaneously in both the clockwise (CW) and counterclockwise (CCW) directions. The

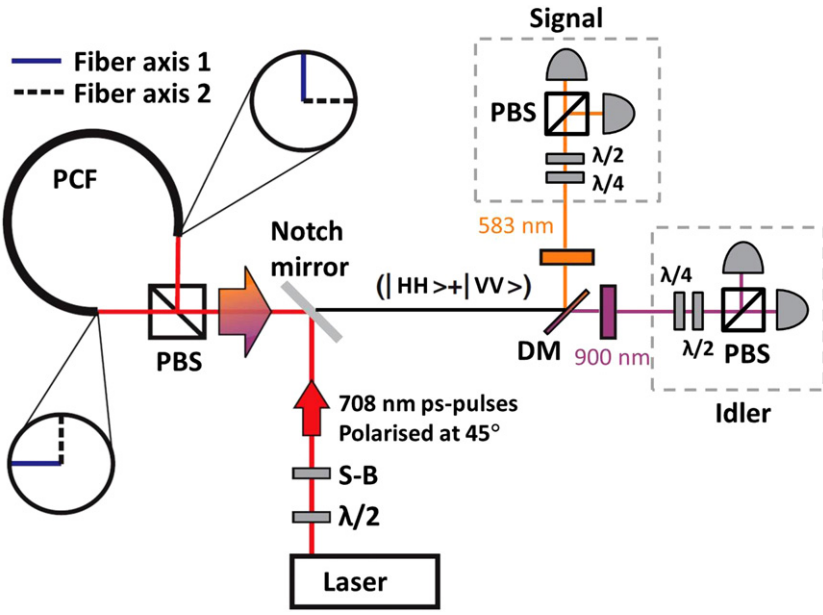

FIGURE 12.20 Schematic representation of a fiber-based entangled photon source setup. A section of PCF forming a Sagnac-loop is pumped in both directions by orthogonally polarized pump pulses, producing entangled pair states when the generated signal and idler pairs are combined onto a single output path. S-B, Soleil-Babinet compensator; PBS, polarizing beam-splitter; DM, dichroic mirror. *Image from [14]. Copyright (year of paper) by the American Physical Society.*

simultaneous pumping is achieved by splitting the pulses from a single pump laser on a polarizing beam-splitter (PBS), and adjusting the polarization state of the laser such that the pump power propagating in both directions through the fiber is balanced. The PBS causes the pump light to be launched into the fiber with a different polarization state for CW and CCW directions, with horizontally polarized (H) pump photons propagating in one direction and vertically polarized (V) pump photons in the other.

If the fiber used for the Sagnac-loop is birefringent, and the fiber is oriented such that the pump photons traveling in both directions are launched with their polarization direction aligned with either the slow or fast birefringent axis of the fiber, then the polarization state of the pump light will remain unchanged as it propagates through the fiber. For a fiber designed to provide phase-matching for co-polarized sFWM, signal and idler photons will be generated predominantly with the same polarization state as the pump. The pump light traveling in one direction around the Sagnac-loop therefore generates H polarized signal and idler photons, while the pump propagating in the opposite direction will generate V polarized signal and idler photons. When the counterpropagating pairs of signal and idler photons meet at the PBS they combine in a coherent

superposition, producing the state

$$|\psi\rangle_{out} = \alpha|H_s H_i\rangle + \beta e^{2i\phi_p}|V_s V_i\rangle, \tag{12.36}$$

upon post-selection of the photons by detection. α and β are weighting terms for the probability of generating HH and VV polarized pairs, which are determined by the proportion of pump power propagating in each direction through the loop, and any polarization dependent losses or variations in collection efficiency. The state shown in Eq. (12.36) also contains a relative phase term between photon pairs in the two polarization states, denoted by ϕ_p. This relative phase is determined by the phase difference between the horizontally and vertically polarized components of the pump beam, and can be easily adjusted through the use of a Soleil-Babinet compensator. By setting $\alpha = \beta = \frac{1}{\sqrt{2}}$ and $\phi_p = 0$, the source can be used to generate the maximally entangled $|\Phi^+\rangle$ Bell state. As with the heralded single-photon sources described in Section 12.3, after the entangled photon state is generated, the signal and idler photons can be separated into different output paths using a prism or dichroic mirror, and then filtered in order to attain a spectrally pure state, and to remove the residual pump light and Raman-scattered photons.

To generate the entangled state shown in Eq. (12.36), subwavelength stability of the relative optical path lengths of the HH and VV photon pairs is required to ensure that the phase ϕ_p is not time-varying. One significant advantage of using a Sagnac-loop arrangement for the generation of entangled photon pairs is that any differences in the optical path length of the loop, due to vibrations or temperature variations for example, affect both the CW and CCW paths equally. This arrangement is therefore inherently phase-stable, and ensures that the path lengths for the HH and VV polarized pairs are balanced.

While the use of a birefringent fiber ensures that the polarization state of pump light propagating in the loop is unaffected by environmentally driven polarization fluctuations, care must be taken to ensure that spectral distinguishability is not introduced between the HH and VV photon pairs. As shown in Section 12.2, even for fibers where birefringence is not required to achieve phase-matching, and the signal and idler photon pairs are generated predominately with the same polarization state as the pump, the presence of a strong birefringence can subtly alter the phase-matching conditions on one axis of the fiber relative to the orthogonal axis. This potential source of spectral distinguishability between the HH and VV pairs can be avoided by incorporating a 90° twist in the fiber loop, so that the pump light is launched onto the same birefringent axis of the fiber in both the CW and CCW directions, ensuring that the phase-matching conditions for both are identical.

With the addition of a 90° twist in the fiber, it is also possible to produce a Sagnac-loop-based source with a fiber designed to generate signal and idler pairs through cross-polarized sFWM with birefringent phase-matching. As described in Section 12.5.1, this regime of phase-matching allows for the generation of

signal and idler photons which are spectrally uncorrelated. An entangled photon source of this type, was described by Clark *et al.* [50], wherein the Sagnac-loop consisted of a 20 cm section of birefringent PCF, designed to generate signal and idler photons near 600 and 860 nm by pumping in the normal dispersion regime of the fiber with a pulsed Ti:Sapphire laser. The dispersion properties of the PCF were designed such that the requirement of asymmetric group velocity matching between the pump and idler wavelengths was satisfied, allowing the entangled signal and idler photon pairs to be generated in an intrinsically pure state.

To demonstrate that entanglement exists between the generated pairs of signal and idler photons from this type of source it is necessary to look for correlations in their polarization states. The detector setup required to perform this measurement is shown in Fig. 12.21, and consists of a PBS, along with a half-wave plate (HWP) and quarter-wave plate (QWP) in order to select the polarization basis in which each photon will be measured, in both the signal and idler output arms of the source. As the settings of these wave-plates are changed, patterns in the rates of coincident detections from single-photon detectors monitoring the output ports of each PBS can be used to reveal the presence of entanglement.

To test for entanglement, the polarization state measurement of one photon of the pair must be made in one of two nonorthogonal polarization bases. For the detector arrangement shown in Fig. 12.21, the most convenient choices are the computational $\{H/V\}$ basis (where the wave plates are set to leave the photon polarization state unchanged, and H and V polarized photons are directed toward alternate detectors) and the diagonal $\{D/A\}$ basis (where the

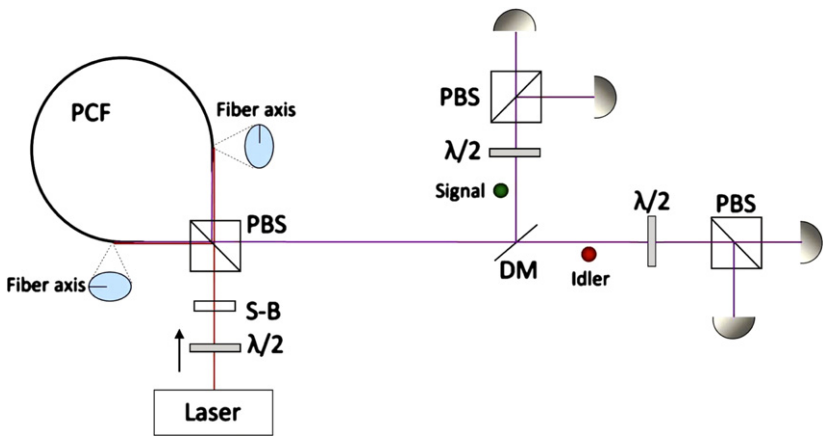

FIGURE 12.21 A setup used to generate entangled photon pairs with a PCF designed for cross-polarized sFWM. The photons can be generated in intrinsically pure spectral states without the need for narrowband spectral filtering. *Image from [50]. ©IOP Publishing Ltd and Deutsche Physikalische Gesellschaft. Published under a CC BY-NC-SA licence.*

HWP rotates the H and V polarization components by 45° relative to the axis of the PBS). While the measurement of one photon of the pair (for instance, the idler) is performed in one of the two fixed bases, the measurement of the other photon (the signal in this example) is carried out across a variety of basis states by rotating the corresponding HWP. The twofold coincidence count rate between one of the signal arm detectors and one of the idler arm detectors is monitored as the signal arm HWP orientation is varied.

Figure 12.22 demonstrates the coincident count rate fringes that would be expected when measuring an entangled state of the type described in Eq. (12.36). In the $\{H/V\}$ basis (with the idler arm HWP set to 0°) high visibility fringes demonstrate that the signal and idler wavelengths are highly correlated. For this choice of measurement basis, this result would also be observed in the classical regime, as each detector can only receive photons generated in either the CW or CCW direction. The polarization state of the detected signal and idler photons are therefore correlated in this case because they are restricted to a fixed linear polarization state by the requirements of phase-matching and the orientation of the birefringent axes of the fiber. When the idler photon is measured in the $\{D/A\}$ basis (idler arm HWP at 22.5°) fringes in the coincidence count rate of the detected signal and idler photons can only be explained by the coherent superposition of the HH and VV photon pairs at the PBS. Perfect visibility of the coincidence fringes in this second nonorthogonal basis would indicate that the photons were maximally entangled, while a flat coincidence count rate without fringes would show that the polarization state of the photons were uncorrelated. A coincidence fringe visibility exceeding 71% indicates that

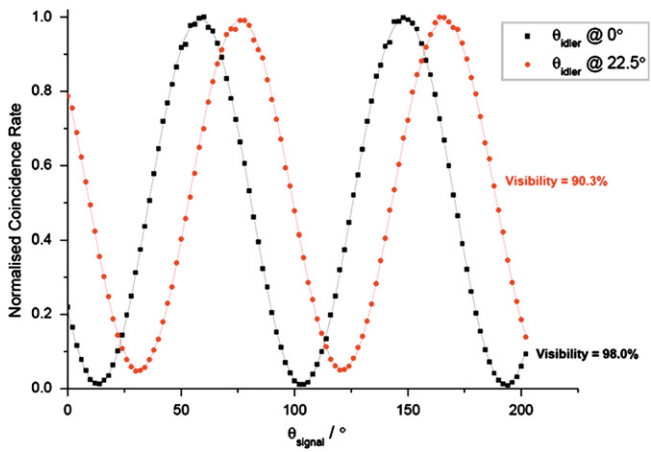

FIGURE 12.22 Measured coincidence count rate data for the entangled photon source described by Clark *et al.* [50]. High visibility fringes can be seen for measurement of the idler in both the {H/V} basis (idler arm HWP set at 0°) and the {D/A} basis (idler arm HWP set at 22.5°), demonstrating the presence of polarization entanglement. *Image from [50].*

the entanglement of the state is sufficient to violate a Bell inequality [72,73], proving that entanglement was present in the generated state. A more detailed analysis of the entangled state can be made using quantum state tomography measurements to reconstruct the density matrix of the photon pair and determine the fidelity with which the experimentally generated state matches that of an idealized maximally entangled state, such as the $|\Phi^+\rangle$ state [74].

Both of the entangled photon source designs described so far in this section were based on birefringent fiber, in order to avoid environmentally driven fluctuations in the polarization state of the propagating pump light and generated photon pairs. An alternative approach that can be used to generate polarization-entangled photon states is based on the technique of polarization-dependent time delay [75]. Figure 12.23 shows such a scheme using a Sagnac-loop, formed by a 50:50 fiber beam-splitter and a section of dispersion-shifted fiber (DSF). In this scheme, two time-delayed, orthogonally polarized pump pulses are launched into one port of the Sagnac-loop. The pump wavelength is carefully chosen to be in the anomalous dispersion regime of the DSF, so that sFWM is phase-matched in the DSF, with the signal and idler wavelengths closely spaced around the pump wavelength. The signal and idler photons are generated predominantly with the same polarization state as the pump; the probability of cross-polarized sFWM occuring is at least one order of magnitude less [76]. At the output of the Sagnac-loop, the initial time delay is removed by passing the two pulses through a piece of polarization-maintaining fiber (PMF) with proper length ℓ satisfying $\ell = \Delta v_g \tau$, where τ is the initial time delay, and Δv_g is the group-velocity difference between light pulses polarized in the PMF's principle states of polarization. At the end of the PMF, there is no way to tell, not even in principle, which pulse generates the signal/idler photon pair in the

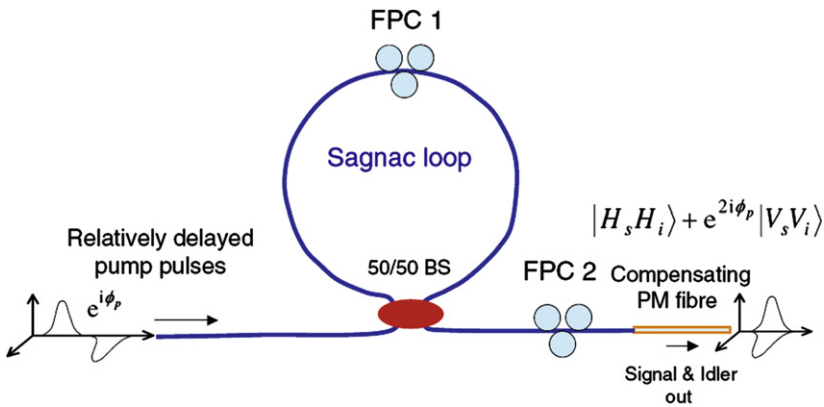

FIGURE 12.23 A simplified schematic of the Sagnac-loop scheme, where most of the experimental details are neglected while putting the emphasis on the gist of the scheme. BS, beam-splitter; FPC, fiber polarization controller; PM, polarization-maintaining. *Image from [16].*

overlapped time slot, and as a result the two probability amplitudes $|H_s H_i\rangle$ and $|V_s V_i\rangle$ are added coherently to give the desired polarization-entangled state $|H_s H_i\rangle + e^{2i\phi_p}|V_s V_i\rangle$, where ϕ_p is the phase difference between the original two pump pulses (ϕ_p can be changed by varying the setting of the polarization-dependent time delay circuit). Note that time-bin entanglement can be created from this scheme if, instead of removing the distinguishing timing information using the PMF at the output, one removes the distinguishing polarization information between the two relatively-delayed time slots.

The reason for using a Sagnac-loop in this scheme is technical rather than fundamental. As described in [77], a properly aligned (by adjusting the intra-loop fiber polarization controller (FPC)) Sagnac-loop can function as a total reflector for the pump photons. In this operational mode, $< 0.1\%$ of the incident pump photons get transmitted through the loop together with the signal/idler photons, and the remaining $> 99.9\%$ of pump photons are reflected back (ignoring the propagation loss of the pump inside the Sagnac-loop). This gives at least 30 dB isolation with respect to the pump in the transmitted mode. Since typically a pump rejection ratio > 100 dB is required to reliably detect the trace amount of signal/idler photon pairs [78], placing a free-space double-grating filter at the output of the PMF can provide the additional $\backsimeq 75$ dB rejection for the pump, satisfying the 100 dB requirement.

A drawback with the setup in Fig. 12.23, however, is that it requires sophisticated phase tracking and locking to maintain a fixed relative phase between the pump pulses. In addition, fiber-birefringence induced polarization fluctuations need to be carefully compensated before sending the photon pairs through the polarization maintaining fiber for accurately removing the time delay. Liang *et al.* demonstrated an ultra-stable, alignment-free setup that eliminates those needs [15]. A schematic of its experimental setup is shown in Fig. 12.24, where the system's principal axes are defined by a four-port fiber PBS. An optical pump-pulse train is prepared at 45° linearly polarized relative to the principal axes and is injected into a fiber circulator which has the basic property of transmitting incident light between its three ports in a successive fashion: light incident on port one is passed to port two and light that returns back into port two is then passed to port three. To avoid unfavorable polarization rotation of the pump pulses, a polarization-maintaining fiber circulator can be used for bringing the pump pulses to the input port of the PBS. At the output ports of the PBS, each 45° linearly polarized pump pulse is decomposed into horizontally and vertically polarized components P_H and P_V, respectively, with a relative phase ϕ_p equal to zero.

P_V is reflected and guided to a Faraday mirror (FM1) at the start of its itinerary: PBS $\rightarrow$ FM1 $\rightarrow$ PBS $\rightarrow$ FM3 $\rightarrow$ PBS $\rightarrow$ FM2 $\rightarrow$ PBS. A Faraday mirror is a non-reciprocal optical element which produces a reflection with a state-of-polarization (SOP) that is orthogonal to the input SOP. Thus, uncontrolled polarization rotations occurring along the incident path are automatically compensated on the return path. In this setup, P_V becomes

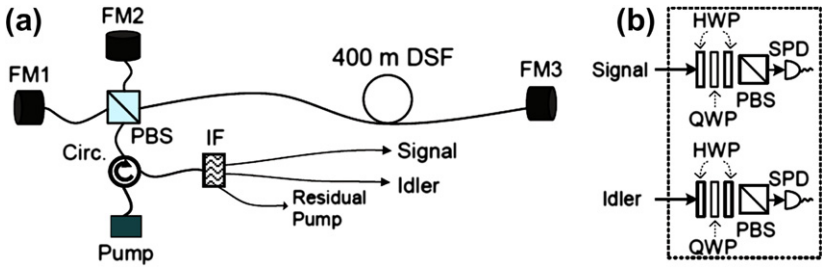

FIGURE 12.24 (a) Schematic setup for an ultra-stable, alignment-free entangled photon source and (b) the polarization control optics and single-photon detectors (SPD) used to verify the generation of entangled photon states. *Images from [15].*

horizontally polarized upon returning to the PBS after reflection from FM1. It then passes through the PBS and enters a 400 m piece of DSF where the sFWM process takes place. Similarly, PH starts its journey PBS $\rightarrow$ FM2 $\rightarrow$ PBS $\rightarrow$ FM3 $\rightarrow$ PBS $\rightarrow$ FM1 $\rightarrow$ PBS by going to FM2. It then arrives back at the PBS vertically polarized and reflects to enter the DSF. A small length difference between the paths to FM1 and FM2 are intentionally designed so that a time delay, which is much greater than the pump pulse duration, is introduced between the arrival times of P_H and P_V at the DSF.

In the DSF, P_H and P_V independently engage in sFWM processes and create signal-idler photon pairs. Note that P_H and P_V experience almost the same insertion loss before entering into the DSF; thus the two sFWM processes have almost the same efficiency. As mentioned above, the signal and idler photon pairs are co-polarized with respect to the pump pulses. With the use of FM3, birefringence-induced polarization fluctuations of the light in the DSF between PBS and FM3 are also automatically compensated. In addition, the polarization states of the two pump pulses and the generated photon pairs are rotated by 90° when they arrive back at the PBS. Hence, P_V and the photon pairs generated from it are directed toward FM2 while P_H and its generated photon pairs travel to FM1. It is easy to see that the information on the generation time of the newly created photon pairs is automatically erased when PH and PV, along with their generated photon pairs, are recombined at the PBS traveling backward through the input port. Upon emerging from the PBS the circulator then directs them away from the pump toward the receivers. With a properly set pump power, the signal and idler photon pairs are emitted in the maximally entangled $\left|\Phi^{+}\right\rangle$ state. It is also important to point out that the pump pulses travel through the DSF twice in this scheme because of FM3. Both P_H and P_V follow a symmetric path through the system. It is this symmetry and the use of Faraday mirrors which automatically compensate any long-term polarization and/or phase fluctuations that enable an ultra-stable and alignment-free source of polarization entanglement. After passing through the circulator, the photon

pairs are separated from the residual pump by fiber interference filters, and are then ready for use in various quantum communication applications. Using this Faraday-mirror setup, generation of entangled photon pairs was demonstrated in both the 1310 nm telecom O-band and the 1550 nm C-band with near-unity fidelity [15,79].

All of the above schemes generate polarization-entangled signal and idler photons of different wavelength. Medic *et al.* demonstrated a source of polarization-entangled photon pairs that is totally degenerate and that deterministically splits each pair of photons into separate single-mode optical fibers [80]. It is built on a "quantum splitter" design for a Sagnac-loop-based source of identical photon pairs [81]. A schematic of the experimental setup is shown in Fig. 12.25, where a dual-frequency, diagonally polarized pump ($|D_p^{(\omega_1,\omega_2)}\rangle$) spontaneously four-wave mixes into two co-polarized, spatially separated, and central-wavelength signal ($|D_s\rangle$) and idler $|D_i\rangle$ photons through $|D_p^{(\omega_1,\omega_2)}\rangle \rightarrow |D_s\rangle|D_i\rangle$, where $|D_j\rangle = (|H_j\rangle\rangle + |V_j\rangle)/\sqrt{2}$, for $j = s, i$. Note that these photon pairs are not polarization entangled. Entanglement generation requires that a distinguishing degree of freedom be coupled to the pump polarization before the sFWM, and that this distinguishing information be subsequently erased, causing orthogonal photon-pair amplitudes to superpose. Consider the diagonally polarized pump $|D_p^{(\omega_1,\omega_2)}\rangle$. After a polarization-dependent time delay (PDD) t', the pump state can be described by $(|H_p^{(\omega_1,\omega_2)}\rangle \otimes |t + t'\rangle + |V_p^{(\omega_1,\omega_2)}\rangle \otimes |t\rangle)/\sqrt{2}$. Here, the PDD is implemented by means of free-space optical delay paths after a polarizing beam-splitter in a Michelson configuration. The degenerate pair production (from reverse HOM interference between the sFWM amplitudes) is then described by

$$|H_p^{(\omega_1,\omega_2)}\rangle \otimes |t + t'\rangle + |V_p^{(\omega_1,\omega_2)}\rangle \otimes |t\rangle) \rightarrow |H_s H_i\rangle \otimes |t + t'\rangle + |V_s V_i\rangle \otimes |t\rangle). \tag{12.37}$$

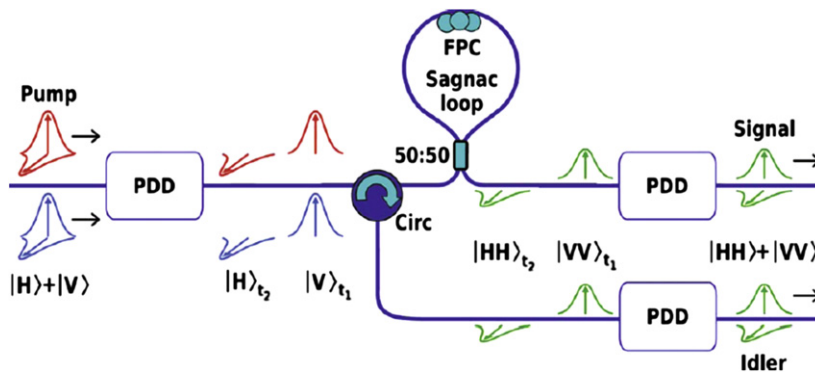

FIGURE 12.25 Setup for generating degenerate, polarization-entangled, and deterministically split photons: PDD, polarization-dependent time delay; FPC, fiber polarization controller; Circ, circulator; $t_2 = t_1 + t'$. *Image from [80].*

By subjecting these degenerate photons to a second set of complementary PDDs the Bell state $\frac{1}{\sqrt{2}}(|H_s H_i\rangle + |V_s V_i\rangle) \otimes |t\rangle$ is produced.

Finally, Chen *et al.* demonstrated a hybrid scheme that combines the benefits of the Sagnac-loop interferometer and the counterpropagating (CP) schemes. It is called a double-loop (DL) scheme, due to the topological fact that there are two loops intertwined with each other, namely, a PBS loop and a Sagnac-loop (see below). Such a DL scheme can be viewed as a perfect combination of the SL and CP schemes. On one hand, the Sagnac-loop in the DL scheme performs exactly the same way as in the Sagnac-loop scheme, which is to provide pump isolation of around 30 dB. On the other hand, the DL scheme is just a modified CP scheme, with the Sagnac-loop replacing the straight-fiber configuration. The strengths of both the SL and CP schemes are successfully retained in the DL scheme, namely, $\backsimeq$ 30 dB built-in filtering capability, easy implementation of a CP-like configuration and suppression of the cross-polarized Raman-scattered photons, as well as photons generated by self-phase modulation of the pump.

A simplified schematic of the DL scheme is shown in Fig. 12.26. Just like in the CP scheme, a 45°-polarized pump pulse splits into two equally powered, orthogonally-polarized components after entering the main loop—the PBS loop. The secondary loop, the Sagnac-loop, is configured as a total reflector for both CW and CCW propagating pumps. In this configuration, $> 99.9\%$ of each pump pulse (ignoring the propagation loss) is reflected back to its original entrance port ($1 \rightarrow 1, 2 \rightarrow 2$), while $< 0.1\%$ of each pump pulse together with its copolarized FWM-generated photon pair gets transmitted ($1 \rightarrow 2, 2 \rightarrow 1$). The FPCs (FPC1 and FPC2) are adjusted such that the following criteria are satisfied:

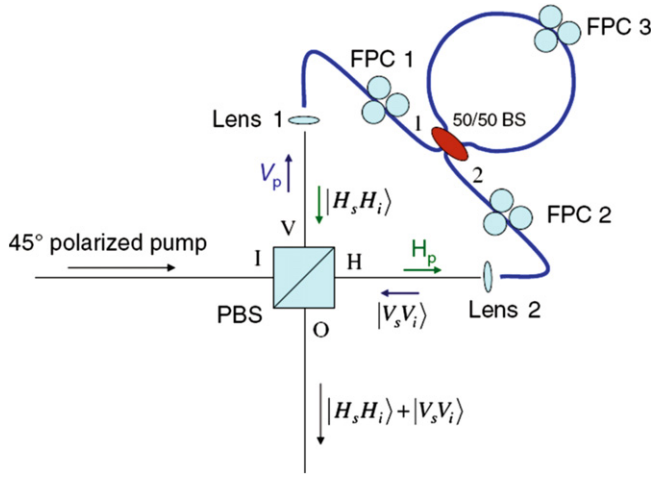

FIGURE 12.26 A simplified schematic of the DL scheme. *Image from [16]. ©IOP Publishing Ltd and Deutsche Physikalische Gesellschaft. Published under a CC BY-NC-SA licence.*

(i) The reflected pump photons maintain their original polarization after their individual round trip (V-port $\rightarrow 1 \rightarrow 1 \rightarrow$ V-port, H-port $\rightarrow 2 \rightarrow 2 \rightarrow$ H-port);

(ii) The transmitted FWM-generated photons, together with the accompanying copolarized pump leakages, regain the initial input polarization after traversing the entire loop (V-port $\rightarrow 1 \rightarrow 2 \rightarrow$ H-port, H-port $\rightarrow 2 \rightarrow 1 \rightarrow$ V-port).

The first criterion is satisfied when all the Sagnac-reflected pump photons go back to the I-port (the input port in Fig. 12.26) of the PBS. The second criterion is satisfied when all the Sagnac-transmitted photons exit from the O-port of the PBS. Due to indistinguishability of the CW and CCW paths, the two coherent FWM-photon amplitudes are thus maximally added to create the desired polarization entanglement, $|H_s H_i\rangle + |V_s V_i\rangle$, with maximum pump isolation provided by the Sagnac-loop. The above seemingly demanding operating conditions were theoretically shown to be feasible. Experimentally, however, it turns out that the first operating criterion can be relatively relaxed without sacrificing the performance of the DL scheme. This is due to the nonoverlapping time slots that the transmitted and reflected pump pulses can be made to occupy when exiting the PBS's O-port. To be more precise, let's denote the light propagation length (including the free-space as well as the fiber) from the PBS's I-port to port 1 of the Sagnac-loop ℓ_1, the Sagnac-loop length L_s, and the light propagation length from port 2 to O-port ℓ_2. The reflected pulse in the CW direction traverses a distance of $2\ell_1 + L_s$, whereas its counterpart in the CCW direction traverses a distance of $2\ell_2 + L_s$. In contrast, the transmitted pulses in both directions traverse the same distance $\ell_1 + L_s + \ell_2$. The pulses' exit-time difference, proportional to their propagation length difference, is thus given by $\Delta t_{\pm} = \pm|\ell_1 - \ell_2|/c$, where the central (or reference) time slot is the overlapping time slot for the transmitted sFWM photons. As can be clearly seen from the above expression for $\Delta t_{\pm}$, one can judiciously choose the propagation length difference to be large enough that the leakage photons from the two reflected pump pulses fall outside the detection-time window for the transmitted photons. This essentially means that even though the first operating criterion may not be satisfied, or a real-life PBS may deviate from its ideal performance, the feasibility of the DL scheme is not sacrificed as long as we choose a suitably long $\Delta t_{\pm}$.

12.7 APPLICATIONS OF FIBER PHOTON SOURCES—ALL-FIBER QUANTUM LOGIC GATES

One application for single and entangled photon states that has generated much interest in recent years is quantum information processing (QIP), with the eventual aim of developing a scalable architecture for quantum computation [82, 70]. Photons have many desirable properties that make them well suited for

use as qubits in QIP applications. The polarization state of a photon provides a convenient system of two orthogonal quantum eigenstates in which a qubit can be easily encoded, as well as manipulated through the use of wave plates and other birefringent optics. Furthermore, due to their incredibly weak interactions with each other and the environment, qubit states encoded on photons are robust against decoherence. Unfortunately, this weak interaction also makes it extremely challenging to realize the type of two-photon operations that are required for computation, where, for example, the state of one qubit is used to conditionally flip the state of another. Currently there are no known materials with sufficiently strong nonlinearity to implement the required phase-shift of π through cross-phase modulation for one single photon to flip the state of another.

In 2001, a seminal paper by Knill *et al.* showed that an effective two-photon interaction could be realized using only linear optical elements through a combination of nonclassical interference and measurement induced nonlinearity [69]. This approach of linear optical quantum computation facilitated the development of two-photon logic gates, of which the controlled-NOT gate (CNOT) is an important example. This logic gate accepts two input photons—known as the control and target qubits. At the output of the gate, the state of the target qubit is conditionally flipped, based on the state of the control qubit, implementing the required two-photon interaction. The CNOT gate, in combination with easily implemented unitary single qubit operations, has been shown to be a universal set of gates for quantum computation, meaning that any conceivable QIP algorithm can be implemented using just these elements [83].

Early experimental implementations of the CNOT gate [84,85] were based on bulk optical elements, making them unsuitable for scaling up to more complex architectures. They also incorporated multiple interferometers, in order to convert the qubits between path and polarization encoding, and therefore required subwavelength path stability for successful operation. Clark *et al.* reported the first experimental demonstration of an optical fiber-based CNOT gate, which overcame many of these limitations [13].

A schematic of the experimental setup, is shown in Fig. 12.27. The setup includes two PCF-based heralded single-photon sources (see Section 12.3). These generate linearly polarized single photons to be used as the control and target polarization encoded qubits. The qubit values are set through the use of HWPs. The CNOT gate itself consists of three partially polarizing fiber couplers (PPFC). The target and control qubit meet at the first PPFC, which is oriented such that the component has reflectivity of $R_H = \frac{1}{3}$ and $R_V = 1$ for H and V polarized photons respectively. If one or both of the input photons are V polarized then there will be no interaction between them and each will be probabilistically reflected or transmitted independently. Successful operation of the gate requires that a single photon is detected in each of the two output channels. If one or both photons are V polarized then both must be reflected at the first PPFC in order for one photon to be detected in each output mode.

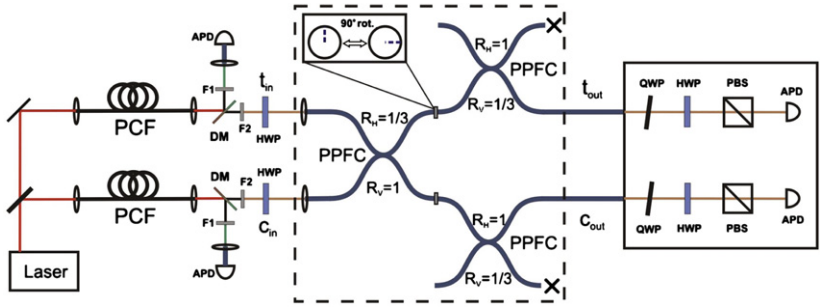

FIGURE 12.27 Experimental setup used to demonstrate an all-fiber CNOT gate. The CNOT gate itself is formed of three partially polarizing fiber couplers (PPFC). Input target and control qubit states (t_{in} and c_{in}) are prepared using two heralded single-photon sources shown on the left-hand side of the figure. The optics shown on the right-hand side of the figure are used to analyze the output states of the target and control qubits after the gate (t_{out} and c_{out}). *Image from [13]. Copyright (year of paper) by the American Physical Society.*

When the input photons are both H polarized and indistinguishable, nonclassical interference will occur between them at the first PPFC. With probability $\frac{1}{9}$ both photons will be transmitted here, giving a π phase-shift for this output state relative to the other possibilities in which both photons are reflected. This interaction therefore implements a controlled phase-shift when both the control and target photons are H polarized at this PPFC. In combination with single qubit rotations of 45° performed by the HWPs on the target qubit at the input and output of the gate, this implements the required CNOT operation [86]. Failure of the gate to function correctly when two H polarized photons are incident on the PPFC results in one of the two output modes being empty. Successful operation of the gate can be verified through post-selection of events in which output target and control photons are detected in coincidence, which occurs with probability $\frac{1}{9}$ in the absence of losses. The other two PPFCs ensure that the success probability of the gate is uniform for all possible input states. A 90° rotation of the birefringent axes of the optical fiber is also incorporated in the setup at the midpoint of the CNOT gate. This compensates for the polarization-mode dispersion that occurs in the birefringent fiber due to the difference in the propagation constant for H and V polarized photons, which would otherwise lead to decoherence of the polarization state for qubits encoded in a diagonal basis relative to the fiber axes.

In order to evaluate the performance of the CNOT gate, wave plates and a PBS placed before each of the single-photon detectors can be used to determine the probability of finding the control and target qubits in a given polarization state at the output of the gate for each of the four possible combinations of logical input states, as shown in Fig. 12.28. This measurement was performed in both the computational basis $\{H/V\}$, where the photon polarizations were aligned with the principal axes of the PPFCs, and in the nonorthogonal diagonal

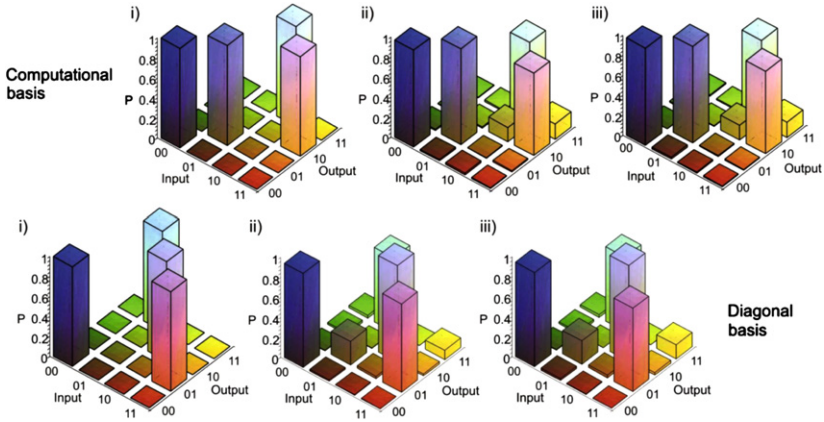

FIGURE 12.28 Truth table results showing the operation performed by the CNOT gate. Results are shown for measurement in both the computational and diagonal bases. The two numbers used to label each input and output state denote the states of the control and target qubits (in that order), with $\{|0\rangle = |V\rangle, |1\rangle = |H\rangle\}$ in the computational basis and $\{|0\rangle = (|H\rangle + |V\rangle)/\sqrt{2}, |1\rangle = (|H\rangle - |V\rangle)/\sqrt{2}\}$ in the diagonal basis. (i) Ideal CNOT gate operation; (ii) experimentally measured values; and (iii) Theoretically modeled predicted values, accounting for imperfect interference visibility. *Image from [13]. Copyright (year of paper) by the American Physical Society.*

basis $\{D/A\}$. Based on these measurements, the classical logical fidelity [87,88] of the all-fiber CNOT gate was calculated to be 0.9 in the $\{H/V\}$ basis and 0.89 in the $\{D/A\}$ basis, and from this the average process fidelity of the gate $\overline{F}$ was found to lie in the range $0.83 \leq \overline{F} \leq 0.91$. It should be noted however that the main limitation on the process fidelity in this case was found to be imperfect quantum interference visibility, resulting from distinguishability between the photons generated by the two independent single-photons sources. Modeling results accounting for this imperfect state preparation showed that the operation of the CNOT gate itself was near-perfect.

This all-fiber implementation of the CNOT gate offers several advantages over bulk optics approaches, including the potential for miniaturization and increased long term stability due to the lack of misalignment issues in a guided wave configuration. In addition, as the gate operates directly on polarization encoded qubits, only a single instance of nonclassical interference is required, without the need for additional classical interferometers. The requirements for the stability of the optical path lengths of the two photons are therefore less stringent, as they only need to be stable to within the coherence length of the photons rather than to a fraction of the photon wavelength. This optical fiber implementation of the CNOT gate is well suited for low loss integration with fiber-based single-photon sources, and paves the way for the development of compact, all-optical fiber QIP circuits.

12.8 PHOTONIC FUSION IN FIBER

Fusion gates are a method for scalably generating large entangled states, which consist of joint measurements applied to pairs of previously unentangled photons [71]. The controlled generation of entanglement is vital to many quantum information applications, including teleportation [89], secret key distribution [90], and most ambitiously quantum computing [82]. Of particular interest is the efficient generation of cluster states, which are a resource for one-way-quantum-computing [91,18]. Once the initial entanglement is generated, the computation can proceed deterministically using a sequence of single qubit measurements.

Figure 12.29a show how overlapping two photons at a PBS can perform a parity measurement. If they are of the same polarization (even parity), they will either both be transmitted or both be reflected, and will leave the beam-splitter in separate modes. This is a successful outcome in that the parity has been measured without gaining any information about the individual polarizations of the photons, and it will leave them in an entangled state. An odd parity outcome leaves both photons at the same output and does not generate entanglement, so the fusion fails 50% of the time. Although this operation is not deterministic, it can be used to build larger states in a scalable way from small entangled states, such as Bell pairs. It is necessary to herald whether the operation has succeeded or failed: in the case of type I fusion (Fig. 12.29a) this is done with a photon-number resolving detector in one of the outputs, so that when the fusion succeeds, one of the photons is detected and destroyed. This allows larger states to be generated in a heralded fashion with some finite probability. Figure 12.29b shows schematically how this can be applied to cluster states—in these pictures, circles represent qubits and bonds represent entanglement between them. Larger states can then be grown in a linear fashion: [71] suggests a strategy of beginning from 5 qubit linear states. Fusing these together, every success adds 4 qubits (because one herald photon is detected and destroyed), while every failed fusion removes 1 qubit. Hence on average the state grows by 1.5 qubits with each fusion.

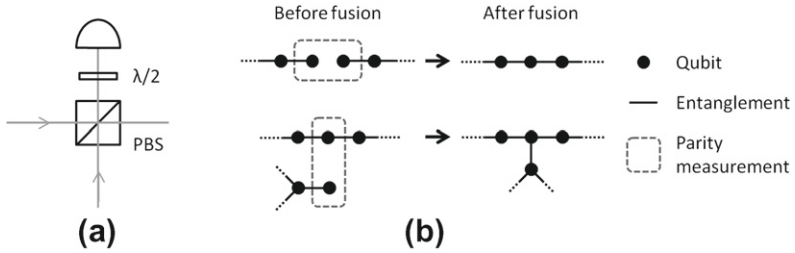

FIGURE 12.29 From [71]. (a) Type I fusion can be used to build long linear cluster states using interference at a PBS. Detection of a photon in one mode heralds the success of the measurement. (b) Linear and 2D cluster geometries produced by fusion operations.

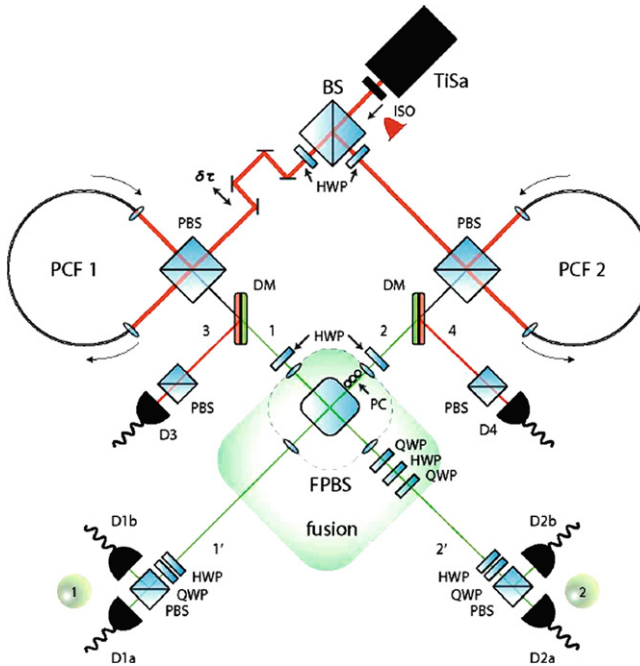

FIGURE 12.30 (a) Type I fusion can be used to build long linear cluster states using interference at a PBS. Detection of a photon in one mode heralds the success of the measurement [71]. (b) Linear and 2D cluster geometries produced by fusion operations. ©IOP Publishing Ltd and Deutsche Physikalische Gesellschaft. Published under a CC BY-NC-SA licence.

Figure 12.30 shows an experimental setup to demonstrate fusion between two photons from separate sources. The input states are prepared using two PCF sources pumped by a pulsed laser. Detections of the idler photons herald the presence of a signal photon from each source. These are both rotated to diagonal polarization, $|D\rangle = \frac{1}{\sqrt{2}}(|H\rangle + |V\rangle)$, so that the state before the fusion gate can be written

$$\frac{1}{2}(|H\rangle_1 + |V\rangle_1)(|H\rangle_2 + |V\rangle_2) = \frac{1}{2}(|HH\rangle_{12} + |HV\rangle_{12} + |VH\rangle_{12} + |VV\rangle_{12}). \tag{12.38}$$

Ideally the fusion operation has the effect of transmitting even parity terms and filtering out odd parity. This can be expressed as

$$|HH\rangle_{12}\langle HH| + |VV\rangle_{12}\langle VV|, \tag{12.39}$$

which, applied to the state in Eq. (12.38), leaves the Bell state $\left|\Phi^+\right\rangle$ with 50% success probability:

$$\left|\Phi^+\right\rangle_{12} = \frac{1}{\sqrt{2}}(|HH\rangle_{12} + |VV\rangle_{12}). \tag{12.40}$$

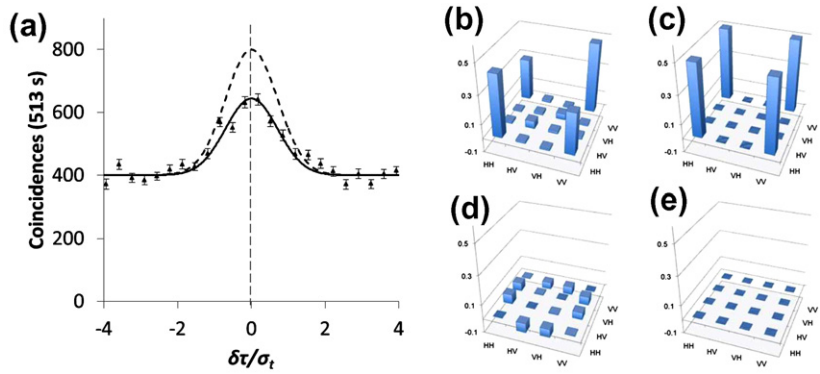

FIGURE 12.31 (a) Increase in DD coincidences when arrival times are matched. The solid line is a fit to the experimental data points and the dashed line shows the ideal case. ©IOP Publishing Ltd and Deutsche Physikalische Gesellschaft. Published under a CC BY-NC-SA licence.

This scheme assumes that the two photons undergoing the fusion are indistinguishable in all degrees of freedom, otherwise they will be left in an incoherent mix of horizontally and vertically polarized pairs [17]. For example, in Fig. 12.30, the arrival time of the photons is matched using a variable delay $\delta\tau$ in one arm. When the output polarization analyzers are set to diagonal, the state should show an increase in the proportion of $|DD\rangle_{12}$ when the photons are indistinguishable—this results from coherent addition of probability amplitudes characteristic of $|\Phi^+\rangle$. This appears as an anti-dip in Fig. 12.31a. The quality of the final state can be characterized more completely with polarization tomography [92,93], as shown in Fig. 12.31b–d.

12.9 CONCLUSION

Spontaneous four-wave mixing in optical fibers is now a well-established approach for realizing probabilistic, nonlinear generation of correlated photon pairs. Signal and idler photons can be generated directly in the guided mode of an optical fiber, allowing them to be easily prepared in both single spatial and polarization modes of a fiber. This makes photon sources based on four-wave mixing well suited for low loss, stable integration with existing single-mode telecommunications fibers. In addition, tight confinement of the interacting guided light fields to the core of a fiber over long lengths allows these sources to demonstrate high brightness in spite of the intrinsically weak nonlinear response of silica.

Sources of heralded single photons and entangled-photon pairs based on four-wave mixing have been demonstrated in both conventional single-mode optical fibers and photonic crystal fibers. Dispersion engineering through design of the fiber structure or the introduction of birefringence can alter the

phase-matching conditions for four-wave mixing, leading to considerable flexibility in the signal and idler wavelengths that can be generated. Further, by tailoring the dispersion appropriately it is possible to generate photons in spectrally uncorrelated, intrinsically pure states without the need for lossy narrowband spectral filtering. The wide variety of two-photon states that can be generated through four-wave mixing makes fiber-based photon sources suitable for many applications including quantum communications, quantum metrology, linear optical quantum computation schemes, and the generation of large entangled cluster states.

As with other photon sources based on the probabilistic generation of photon pairs, the main disadvantage with fiber-based photon sources is the stochastic nature of the pair generation process. This will ultimately limit the scalability of quantum information experiments until methods to efficiently multiplex sources, and to detect and correct for multiple photon-pair generation events, can be further developed. In the short term, moving to low loss, all-fiber schemes should lead to improvements in the brightness of these sources, making quantum information experiments involving higher numbers of photons feasible.

REFERENCES

[1] J.G. Rarity, J. Fulconis, J. Duligall, W.J. Wadsworth, and P.St.J. Russell, "Photonic Crystal Fiber Source of Correlated Photon Pairs," Opt. Express 13, 534–544 (2005).

[2] M. Fiorentino, P.L. Voss, J.E. Sharping, and P. Kumar, "All-Fiber Photon-Pair Source for Quantum Communications," IEEE Photonics Technol. Lett. 14, 983–985 (2002).

[3] J. Fulconis, O. Alibart, W.J. Wadsworth, P.St.J. Russell, and J.G. Rarity, "High Brightness Single Mode Source of Correlated Photon Pairs Using a Photonic Crystal Fiber," Opt. Express 13, 7572–7582 (2005).

[4] A. Ling, J. Chen, J. Fan, and A. Migdall, "Mode Expansion and Bragg Filtering for a High-Fidelity Fiber-Based Photon-Pair Source," Opt. Express 17, 21302–21312 (2009).

[5] A.R. McMillan, J. Fulconis, M. Halder, C. Xiong, J.G. Rarity, and W.J. Wadsworth, "Narrowband High-Fidelity All-Fibre Source of Heralded Single Photons at 1570 nm," Opt. Express 17, 6156–6165 (2009).

[6] C. Söller, B. Brecht, P.J. Mosley, L.Y. Zang, A. Podlipensky, N.Y. Joly, P.St.J. Russell, and C. Silberhorn, "Bridging Visible and Telecom Wavelengths with a Single-Mode Broadband Photon Pair Source," Phys. Rev. A 81, 031801 (2010).

[7] J. Fan, A. Migdall, and L. Wang, "Efficient Generation of Correlated Photon Pairs in a Microstructured Fiber," Opt. Lett. 30, 3368–3370 (2005).

[8] K. Garay-Palmett, H.J. McGuinness, O. Cohen, J.S. Lundeen, R. Rangel-Rojo, A.B. U'Ren, M.G. Raymer, C.J. McKinstrie, S. Radic, and I.A. Walmsley, "Photon Pair-State Preparation with Tailored Spectral Properties by Spontaneous Four-Wave Mixing in Photonic-Crystal Fiber," Opt. Express 15, 14870 (2007).

[9] B. J. Smith, P. Mahou, O. Cohen, J.S. Lundeen, and I.A. Walmsley, "Photon Pair Generation in Birefringent Optical Fibers," Opt. Express 17, 23589–23602 (2009).

[10] M. Halder, J. Fulconis, B. Cemlyn, A. Clark, C. Xiong, W.J. Wadsworth, and J.G. Rarity, "Nonclassical 2-photon Interference with Separate Intrinsically Narrowband Fibre Sources," Opt. Express 17, 4670 (2009).

[11] C. Söller, O. Cohen, B.J. Smith, I.A. Walmsley, and C. Silberhorn, "High-Performance Single-Photon Generation with Commercial-Grade Optical Fiber," Phys. Rev. A 83, 031806 (2011).

[12] M. Patel, J.B. Altepeter, Y.-P. Huang, N.N. Oza, and P. Kumar, "Erasing Quantum Distinguishability Via Single-Mode Filtering," Phys. Rev. A 86, 033809 (2012).

[13] A.S. Clark, J. Fulconis, J.G. Rarity, W.J. Wadsworth, and J.L. O'Brien, "All-Optical-Fiber Polarization-Based Quantum Logic Gate," Phys. Rev. A 79, 030303 (2009).
[14] J. Fulconis, O. Alibart, J.L. O'Brien, W.J. Wadsworth, and J.G. Rarity, "Nonclassical Interference and Entanglement Generation Using a Photonic Crystal Fiber Pair Photon Source," Phys. Rev. Lett. 99, 120501 (2007).
[15] C. Liang, K.F. Lee, T. Levin, J. Chen, and P. Kumar, "Ultra Stable All-Fiber Telecom-Band Entangled Photon-Pair Source for Turnkey Quantum Communication Applications," Opt. Express, 14, 6936–6941 (2006).
[16] J. Chen, K.F. Lee, X. Li, P.L Voss, and P. Kumar, "Schemes for Fibre-Based Entanglement Generation in the Telecom Band," New J. Phys. 9, 289 (2007).
[17] B. Bell, A.S. Clark, M.S. Tame, M. Halder, J. Fulconis, W.J. Wadsworth, and J.G. Rarity, "Experimental Characterization of Photonic Fusion Using Fiber Sources," New J. Phys. 14, 023021 (2012).
[18] M.A. Nielsen, "Optical Quantum Computation Using Cluster States," Phys. Rev. Lett. 93, 040503 (2004).
[19] Dawn Hollenbeck, Cyrus D. Cantrell, "Multiple-vibrational-mode model for fiber-optic Raman gain spectrum and response function," J. Opt. Soc. Am. B 19, 2886 (2002).
[20] W. Wadsworth, N. Joly, J. Knight, T. Birks, F. Biancalana, and P. Russell, "Supercontinuum and Four-Wave Mixing with q-switched Pulses in Endlessly Single-Mode Photonic Crystal Fibres," Opt. Express 12, 299–309 (2004).
[21] B. Ainslie and C. Day, "A Review of Single-Mode Fibers with Modified Dispersion Characteristics," J. Lightwave Technol. 4, 967–979 (1986).
[22] O. Alibart, J. Fulconis, G.K.L. Wong, S.G. Murdoch, W.J. Wadsworth, and J.G. Rarity, "Photon Pair Generation Using Four-Wave Mixing in a Microstructured Fibre: Theory Versus Experiment," New J. Phys. 8, 67 (2006).
[23] J. Chen, X. Li, and P. Kumar, "Two-Photon-State Generation Via Four-Wave Mixing in Optical Fibers," Phys. Rev. A 72, 033801 (2005).
[24] Q. Lin, F. Yaman, and G.P. Agrawal, "Photon-Pair Generation in Optical Fibers Through Four-Wave Mixing: Role of Raman Scattering and Pump Polarization," Phys. Rev. A 75, 023803 (2007).
[25] R.W. Boyd, "Nonlinear Optics", 3rd ed., Academic Press (2008).
[26] C. Xiong and W.J. Wadsworth, "Polarized Supercontinuum in Birefringent Photonic Crystal Fibre Pumped at 1064 nm and Application to Tuneable Visible/UV Generation," Opt. Express 16, 2438–2445 (2008).
[27] A. Ortigosa-Blanch, A. Diez, M. Delgado-Pinar, J.L. Cruz, and M.V. Andres, "Ultrahigh Birefringent Nonlinear Microstructured Fiber," IEEE Photon. Tech. Lett. 16, 1667–1669 (2004).
[28] X. Li, P. Voss, J. Chen, K. Lee, and P. Kumar, "Measurement of Co- and Cross-Polarized Raman Spectra In Silica Fiber for Small Detunings," Opt. Express, 13, 2236–2244 (2005).
[29] H. Takesue and K. Inoue, "1.5 μm Band Quantum-Correlated Photon Pair Generation in Dispersion-Shifted Fiber: Suppression of Noise Photons by Cooling Fiber," Opt. Express, 13, 7832–7839 (2005).
[30] Y.-P. Huang and P. Kumar, "Distilling Quantum Entanglement Via Mode-Matched Filtering," Phys. Rev. A 84, 032315 (2011).
[31] C.K. Hong and L. Mandel, "Experimental Realization of a Localized One-Photon State," Phys. Rev. Lett. 56, 58–60 (1986).
[32] A. McMillan, Development of an All-Fibre Source of Heralded Single Photons, PhD Thesis, University of Bath (2011).
[33] X. Li, J. Chen, P. Voss, J. Sharping, and P. Kumar, "All-Fiber Photon-Pair Source for Quantum Communications: Improved Generation of Correlated Photons," Phys. Rev. Lett. 12, 3737–3744 (2004).
[34] J.E. Sharping, M. Fiorentino, A. Coker, P. Kumar, and R.S. Windeler, "Four-Wave Mixing in Microstructure Fiber," Opt. Lett. 26, 1048–1050 (2001).
[35] J.E. Sharping, M. Fiorentino, P. Kumar, and R.S. Windeler, "Optical Parametric Oscillator Based on Four-Wave Mixing in Microstructure Fiber," Opt. Lett. 27, 1675–1677 (2002).
[36] J.E. Sharping, J. Chen, X. Li, and P. kumar, "Quantum Correlated Twin Photons from Microstructure Fiber," Opt. Express 12, 3086–3094 (2004).

[37] J. Fan, A. Dogariu, and L.J. Wang, "Generation of Correlated Photon Pairs in a Microstructure Fiber," Opt. Lett. 30, 1530–1532 (2005).
[38] J. Fan and A. Migdall, "A Broadband High Spectral Brightness Fiber-Based Two-Photon Source," Opt. Express 15, 2915–2920 (2007).
[39] E.A. Goldschmidt, M.D. Eisaman, J. Fan, S.V. Polyakov, and A. Migdall, "Spectrally Bright and Broad Fiber-Based Heralded Single-Photon Source," Phys. Rev. A 78, 013844 (2008).
[40] J.A. Slater, J.-S. Corbeil, S. Virally, F. Bussières, A. Kudlinski, G. Bouwmans, S. Lacroix, N. Godbout, and W. Tittel, "Microstructured Fiber Source of Photon Pairs at Widely Separated Wavelengths," Opt. Lett. 35, 499–501 (2010).
[41] N. Sangouard, C. Simon, H. de Riedmatten, and N. Gisin, "Quantum Repeaters Based on Atomic Ensembles and Linear Optics," Rev. Mod. Phys. 83, 33–80 (2011).
[42] L. Xiao, M.S. Demokan, W. Jin, Y. Wang, and C.-L. Zhao, "Fusion Splicing Photonic Crystal Fibers and Conventional Single-Mode Fibers: Microhole Collapse Effect," J. Lightwave Technol. 25, 3563–3574 (2007).
[43] T.A. Birks, J.C. Knight, and P.St.J. Russell, "Endlessly Single-Mode Photonic Crystal Fiber," Opt. Lett. 22, 961–963 (1997).
[44] C.K. Hong, Z.Y. Ou, and L. Mandel, "Measurement of Subpicosecond Time Intervals Between Two Photons by Interference," Phys. Rev. Lett. 59, 2044–2046 (1987).
[45] Z.Y.J. Ou, "Multi-Photon Quantum Interference," Springer (2007).
[46] J. Fulconis, O. Alibart, W.J. Wadsworth, and J.G. Rarity, "Quantum Interference with Photon Pairs Using Two Micro-Structured Fibres," New J. Phys. 9, 276 (2007).
[47] A.B. U'Ren, C. Silberhorn, R. Erdmann, K. Banaszek, W.P. Grice, I.A. Walmsley, and M.G. Raymer, "Generation of Pure-State Single-Photon Wavepackets by Conditional Preparation Based on Spontaneous Parametric Downconversion," Laser Phys. 15, 146 (2005).
[48] W.P. Grice, A.B. U'ren, and I.A. Walmsley, "Eliminating Frequency and Space-Time Correlations in Multiphoton States," Phys. Rev. A 64, 063815 (2001).
[49] O. Cohen, J.S. Lundeen, B.J. Smith, G. Puentes, P.J. Mosley, and I.A. Walmsley, "Tailored Photon-Pair Generation in Optical Fibers," Phys. Rev. Lett. 102, 123603 (2009).
[50] A. Clark, B. Bell, J. Fulconis, M.M. Halder, B. Cemlyn, O. Alibart, C. Xiong, W.J. Wadsworth, and J.G. Rarity, "Intrinsically Narrowband Pair Photon Generation in Microstructured Fibres," New J. Phys. 13, 065009 (2011).
[51] A.R. McMillan, M. Delgado-Pinar, J.G. Rarity, and W.J. Wadsworth, "Generation of Narrowband 1550 nm Photons in the Anomalous Dispersion Region of a Birefringent PCF," in Proceedings of the International Quantum Electronics Conference and Conference on Lasers and Electro-Optics Pacific Rim 2011, Optical Society of America, p. I591 (2011).
[52] K. Garay-Palmett, H.J. McGuinness, O. Cohen, J.S. Lundeen, R. Rangel-Rojo, A.B. U'ren, M.G. Raymer, C.J. McKinstrie, S. Radic, and I.A. Walmsley, "Photon Pair-State Preparation with Tailored Spectral Properties by Spontaneous Four-Wave Mixing in Photonic-Crystal Fiber," Opt. Express 15, 14870–14886 (2007).
[53] Z.H. Levine, J. Fan, J. Chen, A. Ling, and A. Migdall, "Heralded, Pure-State Single-Photon Source Based on a Potassium Titanyl Phosphate Waveguide," Opt. Express 18, 3708–3718 (2010).
[54] J.S. Neergaard-Nielsen, B.M. Nielsen, H. Takahashi, A.I. Vistnes, and E.S. Polzik, "High Purity Bright Single Photon Source," Opt. Express 15, 7940–7949 (2007).
[55] P.J. Mosley, J.S. Lundeen, B.J. Smith, P. Wasylczyk, A.B. U'Ren, C. Silberhorn, and I.A. Walmsley, "Heralded Generation of Ultrafast Single Photons in Pure Quantum States," Phys. Rev. Lett. 100, 133601 (2008).
[56] O. Cohen, J.S. Lundeen, B.J. Smith, G. Puentes, P.J. Mosley, and I.A. Walmsley, "Tailored Photon-Pair Generation in Optical Fibers," Phys. Rev. Lett. 102, 123603 (2009).
[57] C. Söller, B. Brecht, P.J. Mosley, L.Y. Zang, A. Podlipensky, N.Y. Joly, P.St.J. Russell, and C. Silberhorn, "Bridging Visible and Telecom Wavelengths with a Single-Mode Broadband Photon Pair Source," Phys. Rev. A 81, 031801 (2010).
[58] Y.-P. Huang, J.B. Altepeter, and P. Kumar, "Heralding Single Photons Without Spectral Factorability," Phys. Rev. A 82, 043826 (2010).
[59] D. Splepian and H.O. Pollak, Bell Syst. Tech. J. 40, 43 (1961).
[60] C. Zhu and C.M. Caves, "Photocount Distributions for Continuous-Wave Squeezed Light," Phys. Rev. A 42, 6794–6804 (1990).

[61] M. Sasaki and S. Suzuki, "Multimode Theory of Measurement-Induced Non-gaussian Operation on Wideband Squeezed Light: Analytical Formula," Phys. Rev. A 73, 043807 (2006).
[62] Y.-P. Huang, J.B. Altepeter, and P. Kumar, "Optimized Heralding Schemes for Single Photons," Phys. Rev. A 84, 033844 (2011).
[63] A. Aspect, P. Grangier, and G. Roger, "Experimental Tests of Realistic Local Theories Via Bell's Theorem," Phys. Rev. Lett. 47, 460–463 (1981).
[64] N. Gisin, G. Ribordy, W. Tittel, and H. Zbinden, "Quantum Cryptography," Rev. Mod. Phys. 74, 145 (2002).
[65] N. Gisin and R. Thew, "Quantum Communication," Nat. Photonics 1, 165–171 (2007).
[66] V. Scarani, H. Bechmann-Pasquinucci, N.J. Cerf, M. Dušek, N. Lütkenhaus, and M. Peev, "The Security of Practical Quantum Key Distribution," Rev. Mod. Phys. 81, 1301–1350 (2009).
[67] H.-J. Briegel, W. Dür, J.I. Cirac, and P. Zoller, "Quantum Repeaters: The Role of Imperfect Local Operations in Quantum Communication," Phys. Rev. Lett. 81, 5932–5935 (1998).
[68] M.P. Hedges, J.J. Longdell, Y. Li, and M.J. Sellars, "Efficient Quantum Memory for Light," Nature 465, 1052–1056 (2010).
[69] E. Knill, R. Laflamme, and G.J. Milburn, "A Scheme for Efficient Quantum Computation with Linear Optics," Nature 409, 46–52 (2001).
[70] J.L. O'Brien, "Optical Quantum Computing," Science 318, 1567–1570 (2007).
[71] D.E. Browne and T. Rudolph, "Resource-Efficient Linear Optical Quantum Computation," Phys. Rev. Lett. 95, 010501 (2005).
[72] J.S. Bell, "On the Einstein-Podolsky-Rosen Paradox," Physics 1, 195–200 (1964).
[73] J.F. Clauser, M.A. Horne, A. Shimony, and R.A. Holt, "Proposed Experiment to Test Local Hidden Variable Theories," Phys. Rev. Lett. 23, 880 (1969).
[74] D.F.V. James, P.G. Kwiat, W.J. Munro, and A.G. White, "Measurement of Qubits," Phys. Rev. A 64, 052312 (2001).
[75] X. Li, P.L. Voss, J.E. Sharping, and P. Kumar, "Optical-Fiber Source of Polarization-Entangled Photons in the 1550 nm Telecom Band," Phys. Rev. Lett. 94, 053601 (2005).
[76] X. Li, P. Voss, J. Chen, K. Lee, and P. Kumar, "Measurement of Co- and Cross-Polarized Raman Spectra in Silica Fiber for Small Detunings," Opt. Express 13, 2236–2244 (2005).
[77] D.B. Mortimore, "Fiber Loop Reflectors," J. Lightwave Technol. 6, 1217–1224 (1988).
[78] M. Fiorentino, P. Voss, J.E. Sharping, and P. Kumar, "All-Fiber Photon-Pair Source for Quantum Communications," IEEE Photonic. Technol. Lett. 14, 983–985 (2002).
[79] M.A. Hall, J.B. Altepeter, and P. Kumar, "Drop-in Compatible Entanglement for Optical-Fiber Networks," Opt. Express 17, 14558–14566 (2009).
[80] M. Medic, J.B. Altepeter, M.A. Hall, M. Patel, and P. Kumar, "Fiber-Based Telecommunication-Band Source of Degenerate Entangled Photons," Opt. Lett. 35, 802–804 (2010).
[81] J. Chen, K.F. Lee, and P. Kumar, "Deterministic Quantum Splitter Based on Time-Reversed Hong-ou-Mandel Interference," Phys. Rev. A 76, 031804 (2007).
[82] M.A. Nielsen and I.L. Chuang, "Quantum Computation and Quantum Information," Cambridge University Press, Cambridge, p. 91 (2000).
[83] M. Fox, "Quantum Optics: An Introduction," Oxford University Press (2006).
[84] J.L. O'Brien, G.J. Pryde, A.G. White, T.C. Ralph, and D. Branning, "Demonstration of an All-Optical Quantum Controlled-Not Gate," Nature 426, 264–267 (2003).
[85] J.L. O'Brien, G.J. Pryde, A. Gilchrist, D.F.V. James, N.K. Langford, T.C. Ralph, and A.G. White, "Quantum Process Tomography of a Controlled-Not Gate," Phys. Rev. Lett. 93, 080502 (2004).
[86] A.S. Clark, Quantum Information Processing in Optical Fibres, University of Bristol PhD Thesis (2011).
[87] H.F. Hofmann, "Complementary Classical Fidelities as an Efficient Criterion for the Evaluation of Experimentally Realized Quantum Operations," Phys. Rev. Lett. 94, 160504 (2005).
[88] R. Okamoto, H.F. Hofmann, S. Takeuchi, and K. Sasaki, "Demonstration of an Optical Quantum Controlled-Not Gate Without Path Interference," Phys. Rev. Lett. 95, 210506 (2005).

[89] C.H. Bennett, G. Brassard, C. Crépeau, R. Jozsa, A. Peres, and W.K. Wootters, "Teleporting an Unknown Quantum State Via Dual Classical and Einstein-Podolsky-Rosen Channels," Phys. Rev. Lett. 70, 1895–1899 (1993).
[90] A.K. Ekert, "Quantum Cryptography Based on Bell's Theorem," Phys. Rev. Lett. 67, 661–663, (1991).
[91] R. Raussendorf and H.J. Briegel, "A One-Way Quantum Computer," Phys. Rev. Lett. 86, 5188–5191 (2001).
[92] U. Leonhardt, "Quantum-State Tomography and Discrete Wigner Function," Phys. Rev. Lett. 74, 4101–4105 (1995).
[93] D.F.V. James, P.G. Kwiat, W.J. Munro, and A.G. White, "Measurement of Qubits," Phys. Rev. A 64, 052312 (2001).